universität wien

# MASTERARBEIT

Title der Masterarbeit

**„Transport of nanopesticides in saturated porous media “**

Verfasser

Daniel Schweizer

angestrebter akademischer Grad

Master of Science (MSc)

Wien, September 2014

| | |
|---|---|
| Studienkennzahl lt. Studienblatt: | A 066 299 |
| Studienrichtung lt. Studienblatt: | Interdisziplinäres Masterstudium Environmental Sciences |
| Betreuer: | Univ.-Prof. Dr. Thilo Hofmann |

## Statutory Declaration

I declare that I have authored this thesis independently, that I have not used other than the declared sources/resources, and that I have explicitly marked all material which has been quoted either literally or by content from the used sources.

Vienna, _____ _____

Date Signature

## Eidesstattliche Erklärung

Ich erkläre an Eides statt, dass ich die vorliegende Arbeit selbstständig verfasst, andere als die angegebenen Quellen/Hilfsmittel nicht benutzt, und die den benutzten Quellen wörtlich und inhaltlich entnommenen Stellen als solche kenntlich gemacht habe.

Wien, am _____ _____

Datum Unterschrift

# Abstract

Polymers, such as Poly($\epsilon$-caprolactone) (PCL), can be utilized to produce core-shell structures (micro- and nanocapsules) acting as containers for an active ingredient (AI) and thereby affecting mobility of the AI in the subsurface. This study was conducted to determine whether PCL based nano-carriers influence transport of the herbicide atrazine through saturated porous media. The effect of a) encapsulation, b) increased ionic strength and c) charge heterogeneity of the collector surface on particle deposition rates and attachment efficiency was investigated using column experiments. The resulting breakthrough curves were fitted and analyzed by solving a convection-dispersion equation implemented in the software STANMOD. Transport and deposition of the particles was described using colloidal filtration theory.

Both, fitting of the breakthrough curves and application of colloid filtration theory revealed no effect of encapsulation on atrazine transport and deposition behavior under unfavorable deposition conditions. However, an increase in ionic strength through addition of the electrolyte $CaCl_2$ did cause a rise in deposition rate and attachment efficiency by about one order of magnitude. As a result deposition of the nanoparticles onto the collector surface was observed ($C/C_0$ = 0.92). By contrast, the subsequent introduction of surface charge heterogeneity through ferrihydite coating of the collector surface did not cause any further change in particle deposition rates or attachment efficiency.

Modeling results and a detected fraction of large particle aggregates ($\geq$1 µm), implied a possible impact of ionic strength on transport behavior by straining. Additionally, initial release rates of the AI were much higher then originally assumed and stated by previous studies [1]. Therefore, the actual particle deposition rate upon increased ionic strength might be substantially higher for the remaining fraction of the encapsulated AI (nanopesticide) than suggested by the particle breakthrough curves.

Furthermore, the results suggest that even though surface charge heterogeneity was not reflected in the calculated particle deposition rate or attachment efficiency, it might prevented either re-entrainment of the nanopesticide or the late release of the AI from already retained nanocapsules.

Overall, the findings of this study indicate that a large fraction of the AI is likely to be transported in solution and would be adequately described by solute transport. Nevertheless, physico-chemical factors (e.g., ionic strength, surface charge heterogeneity) can affect transport and deposition behaviour of the nanopesticide.

Further experiments with nanopesticides exhibiting slower release profiles are needed to capture the impact of nanocapsules on AI transport more sufficiently. Determining the shape of the colloidal spatial distribution within the porous media in combination with a direct measurement technique for the polymer particles at the column outlet could also help to verify straning as a major mechanism for particle retention.

# Contents

**Abstract** iii

**1. Introduction** 1

**2. Material and methods** 5
2.1. Active ingredient . . . 5
2.2. Nanoformulation . . . 6
2.2.1. Preparation of suspensions . . . 7
2.2.2. Release measurement . . . 8
2.2.3. Particle characterization . . . 8
2.3. Porous media . . . 9
2.3.1. Ferrihydrite coating . . . 9
2.3.2. Surface potential . . . 10
2.4. Experimental design . . . 10
2.4.1. Column experiments . . . 10
2.4.2. Tracer . . . 12
2.4.3. Tubing evaluation . . . 14
2.5. Data analysis . . . 15
2.5.1. Particle transport . . . 15
2.5.2. Particle deposition . . . 16
2.6. Statistical analysis . . . 19

**3. Results and discussion** 21
3.1. Nanoparticle characterization . . . 21
3.1.1. Effect of increased particle concentration . . . 23
3.1.2. Effect of increased ionic strength . . . 24
3.2. Porous media characterization . . . 25
3.3. Column experiments . . . 26
3.3.1. Influence of AI encapsulation . . . 26
3.3.2. Influence of increased ionic strength . . . 27
3.3.3. Influence of collector surface charge heterogeneity . . . 29
3.3.4. Transport models and filtration theory . . . 29
3.3.5. Release rates . . . 33

**4. Conclusion** 35

**5. Aknowledgements** **37**

**Bibliography** **39**

## Appendix 45

**A. Zusammenfassung** **47**

**B. Curriculum Vitae** **49**

# List of Figures

1.1. Size domains of colloidal and suspended particles . . . . . 3

2.1. Chemical structure of atrazine . . . . . 5
2.2. Calibration curve of atrazine . . . . . 6
2.3. Experimental setup . . . . . 11
2.4. Calibration curve of the tracer . . . . . 12
2.5. Tracer varification . . . . . 14
2.6. Testing the tubing of the experimental setup . . . . . 14
2.7. Basic transport mechanisms . . . . . 17

3.1. ZetaSizer zeta potential measurements . . . . . 21
3.2. ZetaSizer size measurements . . . . . 22
3.3. EyeTech size measurements . . . . . 23
3.4. Porous media surface charge . . . . . 25
3.5. All breakthrough curves plotted against pore volume . . . . . 27
3.6. All breakthrough curves plotted against time . . . . . 30
3.7. Graphical representation of CFT transport mechanisms . . . . . 32
3.8. Atrazine encapsulation rates . . . . . 33
3.9. Transport and displacement scenarios for the active ingredient . . . 34

# 1. Introduction

With nanotechnology on the rise many new fields of commercial application for engineered nanomaterials are tapped every day. Investments in research and development of nanotechnology are ever rising and some analysts even predict global revenues from nano-enabled products to be worth $2 to 3 trillion by 2015 [2–4]. Already nanomaterials are part of our everyday life and can be found in a variety of products in cosmetics, clothing, electronics, pharmaceuticals and medicine [5, 6].

In recent years, the potential of nanomaterials to offer considerable opportunities for the development of innovative applications and products has also been recognized by the agricultural industry and leading international organizations in this field [7]. Consequently, research activities on nanopesticides as a promising novel plant-protection product has increased extensively [8, 9]. The pest control industry is one of the largest in agriculture [10] and formulations are constantly developed and improved. However, many of the existing active ingredients (AIs) used in widespread pesticide applications are under rising regulatory pressure from governments worldwide due to growing awareness of and concerns about possible negative impacts on human health and the environment [3, 11, 12]. Applying nanoformulations as a nanocarrier to already existing AIs on the market might provide new and enhanced properties and help tackle some of the common, more technical issues experienced with other pesticide formulations [13]. Most prominent goals are the increase of the apparent solubility of poorly soluble AI [9], reduction in quantities required, enhancement of biological activity and better release control. As a side affect, the solution to these problems might actually also encompase an increase in environmental safety of the AI.

Since research on nanoformulations has mainly focused on technical aspects (i.e., stability, biological activity and release mechanisms of nanopesticides), so far little is known about the behaviour and fate of nanopesticides in the environment [14]. However, this information is crucial for a meaningful assessment of the environmental safety and sustainability. Moreover, their fundamental properties and behaviours remain very challenging to assess. This difficulty arises mainly because of their variety in size and shape [4]. Generally nanomaterials are defined as materials with one or more external dimensions or an internal structure at the nanoscale at the order of 100 nm or less [15] which places them into the transition zone between individual atoms or molecules and the corresponding bulk materials [5]. Within this range physico-chemical properties can differ substantially from

the bulk material, due to the increased ratio of surface area to volume and quantum effects that make itself felt [15]. The nanocarriers for agricultural applications usually have internal functional structures at the nanoscale, but outer diameters can easily exceed 100 nm. Even though nanopesticides therefore might not always easily meet size criteria of general nanomaterial definitions, they are still often claimed to exhibit size dependent, novel properties [9].

The anticipated enigmatic behaviour of nanopesticides makes their widespread deliberate introduction into the environment a forseeable source of both new benefits and risks for human health and the environment [16]. Beyond the usually intented goal of improved release control of the AI, nanoformulations may not only influence toxicity and persistence of the AI to the better or worse, but their application as nanocarriers may also considerably enhance or retard transport and leaching into groundwaters [17]. The encapsulation of the AI inevitable increases size of the particle in fluid and modifies acting forces like electrostatical or electrosterical interactions at the interfaces, all affecting transport behaviour [18, 19]. A hydrophobic pesticide could therefore encounter facilitated and much faster movement when associated with a nanocarrier [20], whereas the displacement of a hydrophilic AI might be hindered.

Poly($\epsilon-$caprolactone) (PCL), a hydrophobic, semi-crystalline, biocompatible and biodegradable polymer [21] can be utilized to produce core-shell structures (micro- and nanocapsules) acting as containers for an active ingredient [22]. It has recently been rediscovered as a biomaterial for tissue engineering and targeted release system for drug delivery in medical applications [21]. Grillo *et al.* [1] used PCL to prepare a controlled release system for atrazine which, according to EPA [10] is the second most commonly used herbicide in the US and is applied for agricultural purposes worldwide (70 to 90 million kg annually) [23]. Atrazine is only slightly soluble in water (33 mg $L^{-1}$ at 27 °C, but easily soluble in many organic solvents (36 mg $L^{-1}$ to 183 000 mg $L^{-1}$) [23]. It has been found to contaminate groundwater resources and detected in runoff waters, lakes and streams [23], making it a potential hazard to human health and the environment. As a consequence it has been banned in Germany since 1991 and the European Union in 2004. By applying PCL as a nanocarrier to atrazine, a novel nanopesticide has been designed, which might help minimize negative environmental effects such as groundwater contamination.

Nanoparticles in general and nanopesticides in particular can be placed as a subset of colloidal particles [14], since the conventional definition of the colloidal domain includes particles of up to 1 µm [24, 25] (Figure 1.1).

Colloidal particle transport and their retention in the subsurface environment has a rather high complexity and involves physical and chemical factors interacting at fluid - solid interfaces of both colloids and stationary solid surfaces (collector) [19, 26, 27]. More explicitly, such factors include colloidal traits like size and concentration, but also flow velocity, grain size and pore size distribution of the

media, solution chemistry and surface properties of the collector [28–32].

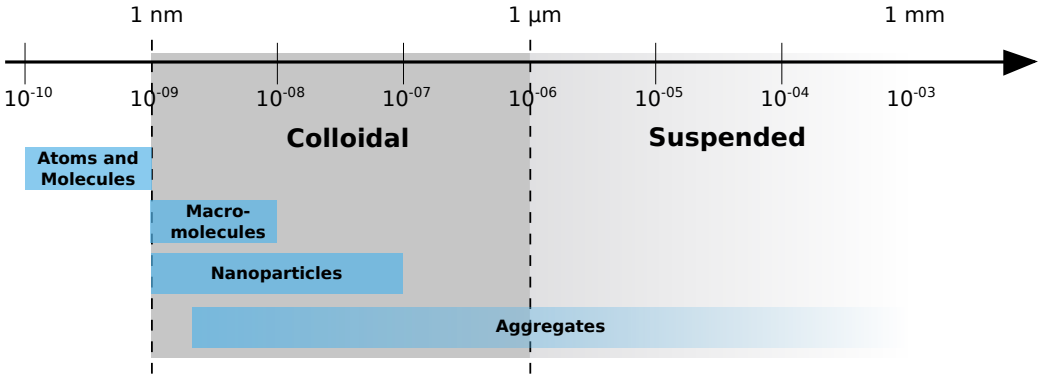


Figure 1.1.: Size domains of colloidal and suspended particles with a classification for nanoparticles, molecules and particle aggregates.[1]

The extent of possible interactions between colloids and collector in a colloidal system, however, is mainly governed by attractive and repulsive forces. They influence particle aggregation, stability and deposition and are a function of the surface charge properties of both porous media and colloids as well as solution chemistry [19]. The Derjaguin-Landau-Verwey-Overbeek (DLVO) theory is commonly applied to calculate and model the components of the interacting forces, of which the most important are the electrostatic double-layer and Van der Waals forces [25]. The repulsive force of the electrostatic double layer is strongly affected by changes in ionic strength, because an increased electrolyte concentration in suspension potentially results in charge screening of the particles as well as cation bridging [14, 33, 34]. The consequential aggregation of particles can greatly affect transport and deposition behavior [25, 35–37].

In general, the deposition of colloids can be described by applying clean bed colloid-filtration theory (CFT). It predicts deposition of suspended particles in a porous media based on a two-step process: (1) transport from the fluid to the grain surface (collector) due to gravitational sedimentation, interception and brownian diffusion and (2) subsequent attachment [26, 28, 38]. As long as attractive forces between colloid and porous media prevail and no energy barrier to attachment exists (favourable conditions) the CFT describes deposition rather well [39].

Polymers such as PCL, which are used for manufacturing of nanopesticides as well as common porous media in the natural environment (quartz, clays) carry a net negative charge at a neutral pH. This can likely result in repulsion and an energy barrier to attachment (unfavorable conditions). Under these conditions collisions between colloids and the solid surface of the collector are not expected to result in irreversible attachment and CFT predictions tend to diverge from

[1] based on Christian *et al.* [14] and Elimelech *et al.* [25]

observed colloid deposition behavior [39–41]. Various attempts have been made to explain the observed discrepancies in deposition, by considering factors not included in the CFT for favorable deposition conditions such as heterogeneous surface charge characteristics of colloids and collector, collector surface roughness, straining [39, 42–44], and deposition of colloids in secondary energy minimum [45].

A collector carrying a heterogeneous surface charge has an increased likelyhood of irreversible attachment, because the energy barrier to attachment is locally reduced or even absent due to a decrease in repulsive interactions [46]. Most natural mineral surfaces express such surface heterogeneities as they are subject to structural variabilities or impurities [17, 47, 48]. Therefore, it can be considered a likely cause of increased deposition rates of colloids (e.g., nanopestices) in natural systems.

The nanopesticide prepared by Grillo *et al.* [1] was used as a case study and applied to a column experimental setup under saturated conditions.

The following study was conducted with the main objective to evaluate the transport behavior of a PCL-based nanoformulation, which carries an AI (i.e., atrazine), in saturated porous media. In detail, the effect of (a) encapsulation, (b) increased ionic strength and (c) charge heterogeneity of the collector surface on particle deposition rates and attachment efficiency is investigated. It is hypothesized that: (a) total transport of the AI is reduced by encapsulation, due to colloidal transport and related deposition mechanisms, (b) increased ionic strength will allow for higher attachment rates, caused by charge screening or cation bridging and, (c) charge heterogeneity will result in an increased likelyhood of particle deposition onto the collector, caused by a local reduction of energy barriers for attachment.

The experimental transport data was further analyzed by simple numerical modeling in order to understand transport behaviour.

# 2. Material and methods

## 2.1. Active ingredient

The herbicide atrazine (2-chloro-4-ethylamino-6-isopropylamino-1,3,5-triazine) was ordered at Sigma-Aldrich (St. Louis, MO, USA) as an analytical standard by PESTANAL (Figure 2.1). With 33 mg $L^{-1}$ at 27 °C it is only slightly soluble in water, but has a wide range of solubility (36 mg $L^{-1}$ to 183 000 mg $L^{-1}$) in organic solvents [23, 49, 50].

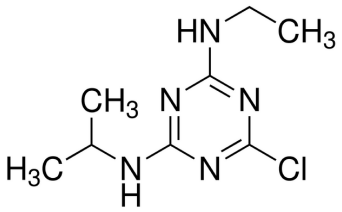


Figure 2.1.: Chemical structure of atrazine.[1]

Due to the hydrophobicity of atrazine, a preliminary stock solution was prepared by dissolving atrazine in 100 % acetonitrile at 1 g $L^{-1}$ using a ultrasonic bath (Sonorex RK 106, ⊘ 240 mm, 130 mm high, 120 W, Bandelin electronic, Germany). For the subsequent application in a transport experiment (*Exp-Atr*) dilution (1:1000, v/v) in deionized water followed, which limited the concentration of the co-solvent acetonitrile to 0.1 % following OECD Guidelines [51], and thereby ensuring minimal impact on the test results. The final atrazine concentration of 1 mg $L^{-1}$ approximately corresponds to typical field application rates of 2.2 kg $ha^{-1}$ to 4.5 kg $ha^{-1}$ [23].

Atrazine concentrations were determined by high performance liquid chromatography (HPLC) equipped with a ZORBAX Eclipse XDB-C18 column (5 µm pore size, 4.6 mm × 150 mm, Agilent). The mobile phase, a mixture consisting of acetonitrile and water (20 % to 80 %) was injected at a flow velocity of 1 mL $min^{-1}$ and 30 °C. Acetonitrile concentration was increased up to 100 % within a 20 min sequence. The variable wavelength detector was set to 230 nm for atrazine quantification at approximately 8 min retention time. Calibration was carried out against a series of

[2]http://www.sigmaaldrich.com/catalog/product/supelco/49085?lang=de&region=DE

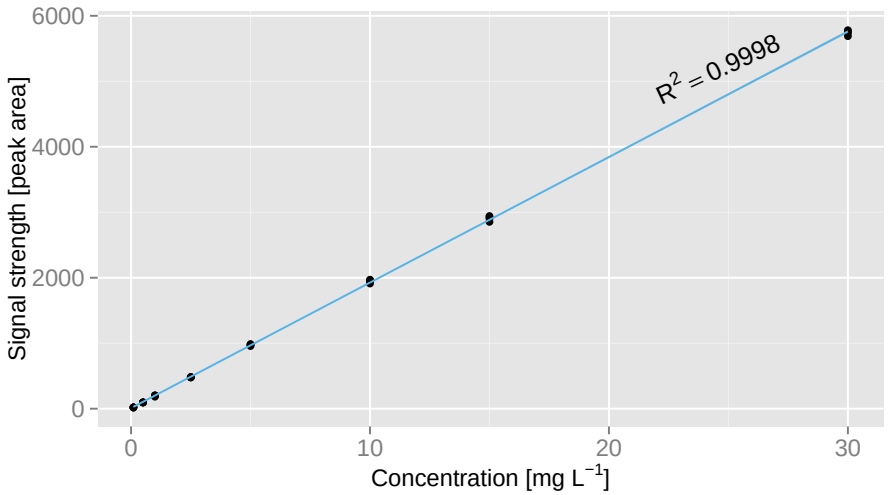


Figure 2.2.: Signal strength (peak area) of the HPLC output against the corresponding atrazine concentration in solution.

eight standards (0.1 mg $L^{-1}$ to 30 mg $L^{-1}$, Figure 2.2) with a limit of quantification (LOQ) of 0.196 mg $L^{-1}$ and a limit of detection (LOD) at 0.059 mg $L^{-1}$.

## 2.2. Nanoformulation

The poly($\epsilon$-caprolactone) (PCL) based nanoformulation of atrazine has been provided by Grillo *et al.* [1] for this study and its preparation is also described exhaustively in Grillo *et al.* [1] and Kah *et al.* [33]. Preparation followed the interfacial deposition of pre-formed polymer method, which employs the mixing of an organic phase into an aqueous phase.

The organic phase was composed of the polymer poly($\epsilon$-caprolactone) with a molecular weight ranging between 70000 and 90000, acetone as an organic solvent, the oil Miglyol 810, which is composed of triglycerides of capric and caprylic acids, a sorbitan monostearate surfactant (Span 60), and the herbicide atrazine [33] (Table 2.1).

The aqueous phase consisted of a solution containing polysorbate 80 surfactant (Tween 80). The components of both phases were dissolved and the organic phase slowly mixed into the aqueous phase, using a magnetic stirrer. After agitation of the resulting suspension, a rotary evaporator was employed to evaporate the organic solvent acetone under reduced pressure. The resulting atrazine concentration of the nanoparticle suspension was approximately 1 g $L^{-1}$ [33].

Table 2.1.: Compounds added to the organic and aqueous phase during preparation of the nanoformulation.

| **Organic phase** | | **Aqueous phase** |
|---|---|---|
| Poly($\epsilon$-caprolactone)[2] | Span 60[3] | Tween 80[4] |
| 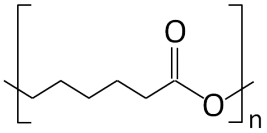 | 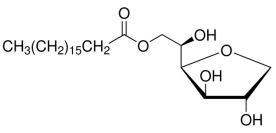 | 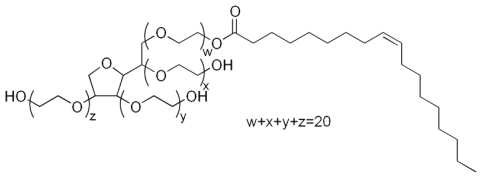 |
| Miglyol 810[5] | Acetone[6] | |
| 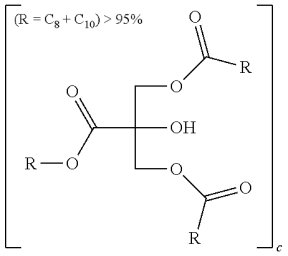 | 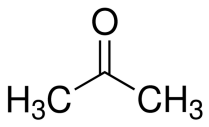 | |

## 2.2.1. Preparation of suspensions

Three different nanoformulation (NF) suspensions were prepared for the transport experiments and particle characterization (Table 2.2). First of all, to acquire a NF suspension with comparable atrazine concentration as employed for the pure atrazine transport experiment (Exp-Atr, 1 mg $L^{-1}$ atrazine), the previously described 1 g $L^{-1}$ NF stock solution was diluted (1:800, v/v) with deionized water ($NF_1$). A second suspension of 10 mg $L^{-1}$ NF concentration was prepared in order investigate any possible effect of increased particle concentration on particle characteristics ($NF_{10}$). However, it was neither intended nor was it expected to significantly affect transport or particle deposition behavior.

Furthermore, to quantify changes in transport and deposition behaviour of the nanopesticide due to increased ionic strength, 10 mmol of $CaCl_2$ was added to another 1 mg $L^{-1}$ NF suspension ($NF_{10}$+$CaCl_2$) and used for the column experiments *Exp-*$NF_{CaCl_2}$ and *Exp-*$NF_{Iron}$). The raise in nanoparticle concentration from 1 mg $L^{-1}$ to 10 mg $L^{-1}$ NF for a portion of the suspensions ($NF_{10}$+$CaCl_2$) used in

[3]http://de.wikipedia.org/wiki/Polycaprolacton
[4]http://www.sigmaaldrich.com/catalog/product/sigma/s7010?lang=de&region=DE
[5]http://de.wikipedia.org/wiki/Tween_80
[6]http://www.google.com/patents/US20130309176
[7]http://de.wikipedia.org/wiki/Aceton

Table 2.2.: Suspensions prepared for particle characterization and column experiments.

| **Suspensions** | **Atrazine** mg $L^{-1}$ | **NF** mg $L^{-1}$ | **$CaCl_2$** mmol $L^{-1}$ |
|---|---|---|---|
| $NF_1$ | 1.14 | 1.25 | 0 |
| $NF_{10}$ | 9.66 | 10.00 | 0 |
| $NF_{10}$+$CaCl_2$ | 9.66 | 10.00 | 10 |

the column experiments was justified by the higher quantity of desired aggregated particles upon addition of the electrolyte $CaCl_2$.

## 2.2.2. Release measurement

The release of the active ingredient atrazine from the nanoformulation into solution was determined using a device consisting of a Swinney Syringe Holder (13 mm, SST, Millipore®, Germany) with an Anodisc filter (0.02 µm, 13 mm, Whatman®, England). The suspensions were manually pressed through the filter device using a glass syringe (10 mL, Metal Luer Lock, ISPG®, USA), separating the AI still encapsulated in the NF by size limited retention on the filter from the AI in solution. The resulting effluent samples comprised approximately 1.5 mL of filtered suspension. All samples were taken within one hour after sample preparation and analyzed by HPLC for total atrazine concentration. Measurements were conducted for a pure atrazine solution (1 mg $L^{-1}$ atrazine) and compared with the $NF_1$ and $NF_{10}$+$CaCl_2$ suspensions.

## 2.2.3. Particle characterization

Size distribution and zeta potential were measured for the three previous suspensions ($NF_1$, $NF_{10}$ and $NF_{10}$+$CaCl_2$, please see section 2.2.1).

### Zeta potential

The zeta potential is an important parameter for the assessment of colloidal stability, because it characterizes electrostatic interactions within colloidal dispersions [52]. In order to determine the zeta potential of the dispersed nanoparticles, Laser Doppler Micro-electrophoresis (Zetasizer Nano ZS, Malvern Instruments, UK) was used.

#### Size distribution

According to Grillo *et al.* [1] the PCL based nanopesticide is expected to be spherical with a rather uniform size distribution and not likely to aggregate. However, addition of $CaCl_2$ was expected to have an impact on particle stability and cause aggregation, resulting in a broader particle size distribution. Therefore, nanoparticle size was determined using two separate measurement techniques for different size ranges.

Dynamic Light Scattering (DLS) is used for small particle diameters measurements between 0.3 nm and 10 µm and converts the diffusion of particles moving under Brownian motion into size and size distribution of particles, applying the Stokes-Einstein relationship (Zetasizer Nano ZS, Malvern Instruments, UK). Samples were analyzed using PMMA cuvettes and post-processed with the general purpose method of the Malvern ZetaSizer software (v703-PSS0012-34-EN-JP).

For larger particles between 0.1 µm to 3600 µm a technique analyzing the laser obscuration time of particles was employed (EyeTech, Ambivalue, The Netherlands). Particle diameters are directly related to the time it takes a laser beam with a fixed velocity to interact with a suspended particle, and produce a shadow on the detector. Hereinafter, diameters of the size analysis are described as both, a function of number and volume. The later is a more accurate measure for describing mean size of suspensions with a significant proportion of larger particles, because the overall contribution to the mean size is weighted by volume and not number.

## 2.3. Porous media

Glass beads (0.15 mm to 0.25 mm) were used as porous media and collector surface. The beads were pre-cleaned to eliminate any impurities by soaking them in 32 % hydrochloric acid (HCL) mixed with deionized water (1:1, v/v) for 24 hours. Subsequent thorough rinsing with deionized water ensured complete removal of any fine material or other residues. The glass beads were then air tried and stored in an airtight container.

### 2.3.1. Ferrihydrite coating

The pre-cleaned glass beads were coated with ferrihydrite in order to increase surface charge heterogeneity towards a more positive zeta potential and, therefore maximize the likelyhood of colloid attachment to the collector. A preparation manual by Cornell & Schwertmann [53] for a synthetic 2-line ferrihydrite coating was modified and adapted. Briefly, 700 mL of 0.06 mol $FeCl_3 \times 6\ H_2O$ was titrated to pH 7 with 2.5 mol NaOH under vigorous stirring and maintained under these conditions for two hours. Afterwards the solution was centrifuged at 3300 g and

excess liquid decanted several times before 240 g of pre-cleaned glass beads were added. The centrifuge procedure was repeated with the resulting mixture. After each run, excess ferrihydrite paste on top of the glass beads was stirred back into the mixture and centrifuged again until no ferrihydrite accumulates were left. The resulting coated glass beads were washed thoroughly with deionized water, dried at room temperature for 72 hours and stored at 4 °C.

The amount of iron oxide precipitated on the glass beads was determined by digesting 2 g of coated glass beads for 45 min in an heated ultrasonic bath (70 °C) using 1 mL of 65 % subboiled Nitric acid and 3 mL of 35 % HCl (Aqua Regia). The liquid phase was then filtered and separated from the beads to be analyzed by inductively coupled plasma optical emission spectrometry (ICP-OES, Optima 5300DV, PerkinElmer, USA). The resulting average amount of iron found per mass of glass beads was 0.670 g $kg^{-1}$.

### 2.3.2. Surface potential

The zeta potentials of the porous media (Figure 3.4) was determined by measuring the streaming potential and streaming current using an Electrokinetic Analyser (SurPass, Anton Paar, Austria). Prior to each measurement the cylindrical measuring cell containing the glass beads sample was equilibrated by flushing it with the background solution in alternating directions for approximately 15 min, ensuring homogeneous flow through the cell in both directions. In congruence with the experimental design the streaming potential was measured using a background solution containing either 1 mmol NaCl or 10 mmol $CaCl_2$ as well as for glass beads coated with Ferrihydrite.

## 2.4. Experimental design

### 2.4.1. Column experiments

A column experimental setup as depicted in Figure 2.3 was used for all transport experiments. It consisted of chromatography borosilicate glass columns (25 mm x 150 mm, 006SCC-25-15-AA, Omnifit®-Labware, Germany), polytetrafluoroethylene (PTFE) tubing (OD = 1/16", Fittings Kit, Omnifit®, Germany) and Tygon® 2001 peristaltic tubing (ID = 0.64 mm, SC0816, Ismatec®, Germany), which were employed in order to keep sorption of the compounds to the experimental setup down to a minimum (Figure 2.6). A peristaltic pump (Ismatec®, Germany) was connected upstream of the column for injection, applying a steady flow rate of 0.1 mL $min^{-1}$ corresponding to a flow velocity of $v_f \approx 3.4 \times 10^{-6}$ m $s^{-1}$. All experiments were simultaneously run in duplicates with two parallel column setups and therefore, data reported in this study is presented as the mean of both.

Nylon Net Filters (Hydrophilic, 180 µm, 25 mm, NY8H02500, EMD Millipore®) were inserted at both inlet and outlet of the glass columns to prevent wash out of the porous media. Their tight and optimal fit inside the column caps resulted in negligible dead volumes and also avoided air bubbles at the perimeters of the caps. Baffles are sometimes used to ensure uniform flow patterns into and out of the column [54]. No baffle was used here, because the impact on transport conditions should be negligible, owing to the homogeneity of the porous media (glass beads) employed.

To account for the dead volume within tubing, the tubing volume was determined and subtracted from the total water volume of the final experimental setup, giving the actual packed glass column pore volume (PV) relevant to all further calculations.

Columns were wet-packed to a bed thickness of 10 cm with glass beads as porous media following the recommended 1:4 diameter to length ratio by Lewis & Sjöstrom [55]. In order to ensure homogeneous and reproducible packing, glass beads were added step-wise. Each step consisted of: 1) pouring 1 cm of media into the column, 2) submerging it with the appropriate background solution (deionized water or 10 mmol $CaCl_2$) later used during the experiment and 3) subsequent stirring and tapping with a spatula. The resulting average density of the matrix was 1.54 kg m$^{-3}$ with a PV of $20.07 \pm 0.62$ mL and a porosity of $40.89 \pm 1.26$

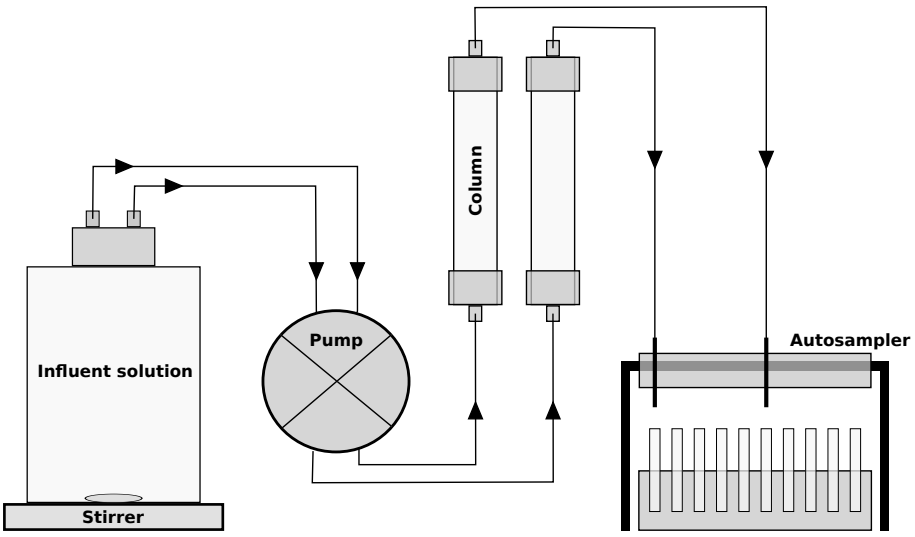


Figure 2.3.: Experimental column setup, with arrows indicating the direction of flow.

Prior to each experiment the porous media was then flushed with at least 2 PV of background solution (deionized water or 10 mmol $CaCl_2$) and to equilibrate the system and ensure minimal background turbidity.

The injection phase of the nanoparticles and atrazine was set to 24 hours equaling approximately 7 PV. This was followed by an elution phase of approximately

12 hours (3.5 PV) where the porous media was flushed with background solution (deionized water or 10 mmol $CaCl_2$).

Samples were collected at the outlet of the column at predefined intervals (15 min and 60 min). Sampling rates were higher (every 15 min) for the first two PV of each experimental phase (injection and elusion) to provide increased resolution. The results of the transport experiments were plotted as breakthrough curves (BTC). The relative concentration ($C/C_o$) was obtained by normalizing the effluent concentrations by the influent concentrations to be then plotted as a function of the PV (time multiplied by flow rate and divided by the water volume inside of the column).

It was neither possible to directly measure the actual effluent concentration of the nanoformulation, nor to distinguish between the amount of atrazine encapsulated by the nanocarrier (PCL polymer) and the amount already freely in solution. Therefore, total effluent atrazine concentration was used as an approximation for transported nanoformulation in all column experiments not taking into account atrazine release rates or encapsulation efficiency [1]. Total atrazine concentrations were determined by HPLC as described above.

### 2.4.2. Tracer

Three different compounds (NaBr, $NaNO_3$ and Fluorescein) were tested in order to identify a suitable conservative tracer that could also be analyzed by high performance liquid chromatography (HPLC) determining total atrazine and tracer concentrations of each collected column sample simultaneously.

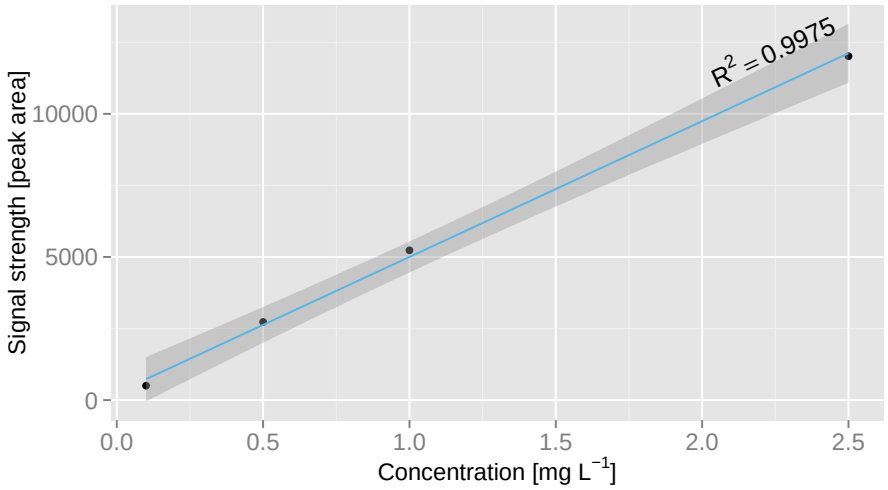


Figure 2.4.: Signal strength (peak area) of the HPLC output against the corresponding $NaNO_3$ concentration in solution.

Fluorescein as a tracer was prone to photodegradation and therefore not reliable enough for application in a long term column experiment. NaBr, a conservative tracer commonly used in column transport experiment [35] also showed degradation over the relevant time interval of 36 hours and was consequently ruled out.

Nitrate ($NaNO_3$) was easily detectable by HPLC (detailed instrumental setup description in section 2.1) and calibration curves showed a reasonable linear relationship ($r^2 = 0.9975$) between tracer concentration and signal strength (peak area) with a slight divergence towards higher concentrations (Figure 2.4). Therefore, $NaNO_3$ was chosen and applied as a conservative tracer during the injection phase of all conducted transport experiments. Concentration was set to 1 mmol $L^{-1}$ and the resulting breakthrough curves were further used to calculate PV and porosity of the porous media using the following equations:

$$PV = \left(\left(\left(\frac{t_1 - t_0}{(C/C_0)_1 - (C/C_0)_0}\right) \times (0.5 - (C/C_0)_0)\right) + t_0\right) \times v_f\right) - TV \quad (2.1)$$

$$n = \frac{PV}{h_c \pi r^2} \quad (2.2)$$

where TV is the tubing volume of the experiment, $t_0$ and $t_1$ are the two points in time (from collected data) before and after 50 % of the breakthrough was measured, $(C/C_0)_0$ and $(C/C_0)_1$ are the corresponding relative concentrations and $h_c$ and $r^2$ are height and radius of the column, respectively.

### Tracer verification

A separate set of experiments was conductedin order to verify $NaNO_3$ as a suitable tracer and confirm the coherence of the previously obtained relationship between the HPLC signal strength and tracer concentrations in solution. Bromide (2 mmol), a typical conservative tracer was, together with $NaNO_3$ (2 mmol), injected into a simplified version of the experimental setup, which only included the tubing but not the columns.

The collected samples were analyzed by ion chromatography (ICS-1000, Dionex, Austria) and by HPLC. The breakthrough curve of the conservative tracer NaBr served as a reference base and matched the breakthrough curves of $NaNO_3$, both measured by IC and HPLC (Figure 2.5). Therefore, the observed congruence of the transport behaviour of NaBr and $NaNO_3$, varifies $NaNO_3$ as a suitable tracer. Additionally, HPLC produces comparable measurement results to the IC method, which confirms its applicability.

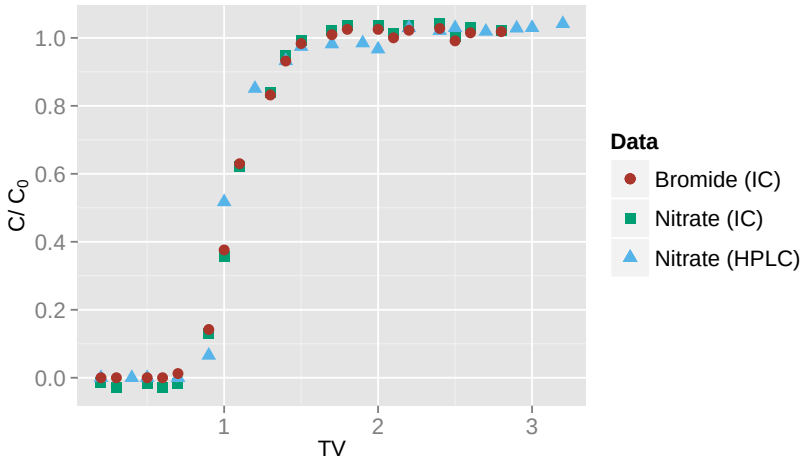


Figure 2.5.: Breakthrough curves of the tracer $NaNO_3$ (Nitrate) and Bromide measured by HPLC and IC. They are plotted as normalized concentration ($C/C_0$) versus number of tubing volumes (TV).

### 2.4.3. Tubing evaluation

To ensure minimum deposition of the nanopesticide or atrazine itself onto any constituents of the experimental setup and thereby affecting the measured effluent concentration, the capacity of the tubing for deposition was evaluated.

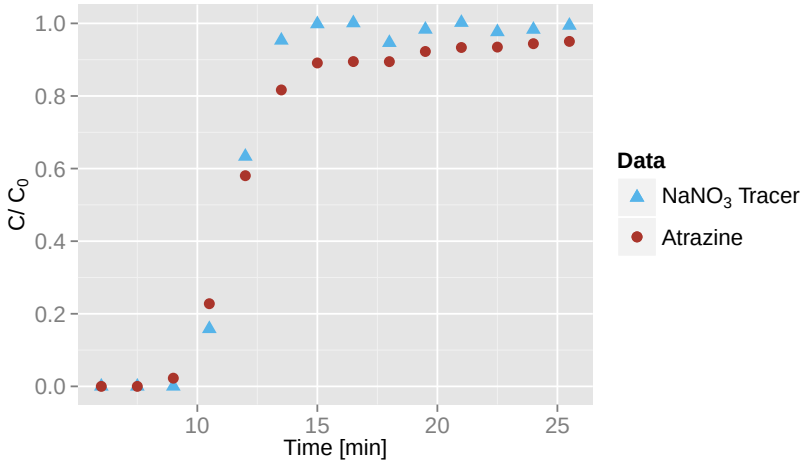


Figure 2.6.: Breakthrough curves of atrazine and $NaNO_3$ plotted against time to check the tubing of the experimental setup.

The $NF_{10}$+$CaCl_2$ suspension also used for particle characterization containing 10 mmol $CaCl_2$, 10 mg $L^{-1}$ of the nanopesticide formulation and 1 mmol $NaNO_3$ (tracer) was applied at a flow rate of 0.1 mL $min^{-1}$ to a modified setup consisting

of the tubing constituents only. Out of several materials being tested the polytetrafluoroethylene (PTFE) tubing and Tygon® 2001 peristaltic tubing showed the best performance (Figure 2.6), because atrazine expressed a nearly conservative transport behavior. Hence those tubing materials were employed during all following experiments. A slight deviation in normalized atrazine concentration when compared to the tracer was observed, however after about 2 tubing volumes the breakthrough leveled out and stabilized at the maximum concentration ($C/C_o = 1$).

## 2.5. Data analysis

### 2.5.1. Particle transport

#### Governing equations

Assuming steady flow through saturated porous media, the one-dimensional transport of particles can be mathematically described by the convection-dispersion equation (CDE). A term for a first-order decay coefficient ($k_{prm}$) is added to account for the overall process of particle removal [56, 57]:

$$\frac{\delta C}{\delta t} = D\frac{\delta^2 C}{\delta x^2} - v\frac{\delta C}{\delta x} - k_{rem}C \tag{2.3}$$

where $C$ is the volume-averaged concentration in the liquid phase, $v$ is the pore water velocity, $t$ the elapsed time, $x$ the distance traveled by the particle, $D$ the corresponding hydrodynamic dispersion coefficient as defined in equation 2.4) by Logan [58] and Scheidegger [59], and $k_{rem}$ is the first-order particle removal rate coefficient. The relevant parameters can mathematically be expressed as follows:

$$D = \alpha_L v + n_e D_{aq} \tag{2.4}$$

$$v_a = \frac{q}{n} \tag{2.5}$$

$$k_{rem} = \frac{\mu q}{L} \tag{2.6}$$

where $\alpha_L$ is the longitudinal dispersivity, $n_e$ the effective porosity, $n$ the porosity, $D_{aq}$ the aqueous diffusion coefficient, $q$ the darcy velocity, $\mu$ a first-order degradation coefficient and $L$ the length of the column.

### Modelling approach

The STANMOD software (CXTFIT, version 2.08.1130) employs the convection-dispersion equation to model theoretical transport of particles in laboratory and field scale experiments. By fitting mathematical solutions of the transport model to the breakthrough curves of the column experiment, the relevant transport parameters can be derived. More explicitly, an objective function is minimized, applying a nonlinear-squares inverse method based on the sum of squares difference between observed and fitted concentrations for each data point of the breakthrough curves [60]. The program was used to estimate the model parameters $D$ and first-order degradation coefficient $\mu$, with the corresponding pore water velocity ($v$) added to the model as a fixed input parameter. To obtain $k_{prm}$ from $\mu$, equation 2.6 was applied.

### Mass balance

The total amount of atrazine collected from all effluent samples ($AI_{Out}$) during each column experiment was calculated and compared to the total amount of atrazine injected into the column experiment ($AI_{In}$) to estimate the quantity of atrazine irreversibly retained in the column after flushing it with the background solution (elusion phase). The resulting recovery rate ($rec_{AI}$) was calculated as follows:

$$AI_{In} = C_s \times t_{tot} \times v_f \tag{2.7}$$

$$AI_{Out} = \sum_{i=1}^{n} C_i \times t_i \times v_f \tag{2.8}$$

$$rec_{AI} = \frac{Atr_{Out}}{Atr_{In}} \tag{2.9}$$

where $C_s$ is the atrazine concentration in suspension, $t_{tot}$ equals the time of the injection phase and $C_i$ as well as $t_i$ are sample specific atrazine concentration and sampling time for all samples (n) of each experiment.

## 2.5.2. Particle deposition

Deposition of particles in suspension onto a stationary solid surface (collector) can be characterized by clean bed colloid-filtration theory [38, 45](see section 1). Assuming a perfect sink model, where all collisions between colloidal particles

and a collector result in attachment (favorable conditions), their transport from the pore fluid to the vicinity of the collector can typically be described by three mechanisms: (1) gravitational sedimentation ($\eta_G$), (2) interception ($\eta_I$) and (3) brownian diffusion ($\eta_D$) (Figure 2.7).

Transport due to gravitational sedimentation refers to a density driven settling of particles onto the collector surface, which occurs if the density of the suspended particle is greater than that of the fluid. A particle moving along the trajectory of a streamline can also simply be intercepted by the collector when they come into contact. Transport of smaller particles such as nanoparticles is strongly governed by brownian motion and the resulting random moving pattern can lead to contact and subsequent attachment as well.

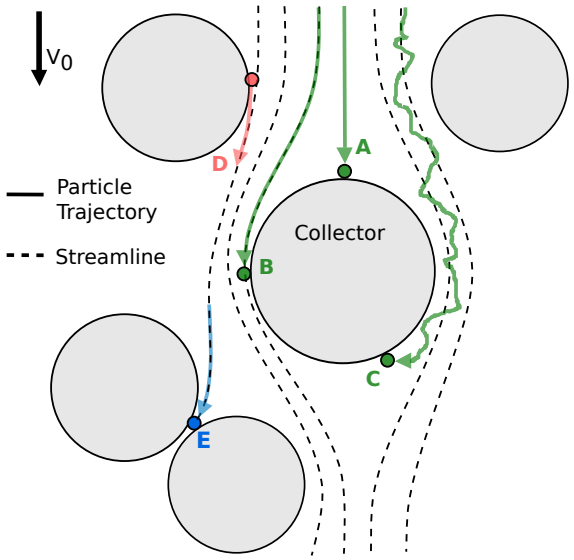


Figure 2.7.: The basic transport mechanisms of physiochemical filtration: (A) sedimentation, (B) interception, (C) diffusion, and (D) detachment as well as the mechanical filtration mechanism (E) straining.

Detachment and re-entrainment of retained particles can be caused by an external input of kinetic energy through increased flow velocity or heat, but also through changes in physiochemical conditions (e.g. drop in ionic strength), that affect the balance of the counteracting forces in the secondary minimum [31, 40]. Flow velocity is constant for the duration of each column experiment, however detachment and re-entrainment can be observed during the elusion phase of the experiments. Especially straining as a physical retention parameter has probably been underestimated in it's importance in colloid transport. Straining can be described as the trapping of colloids in the dead ends of pore spaces, which are too small to allow passage of the particles. Geometric models indicate that those dead ends are more likely to occur when the ratio of particle diameter to collector diameter is greater than 0.002-0.008 [29, 46] with both angular shaped grains

and surface roughness contributing to the porous media straining potential [61]. Since particle size measurements revealed the existence of a size fraction of larger particles ($\geq$1 µm, ratio of particle to collector diameter $\geq$0.005), the possibility of straining to occur and affect particle transport, is to be considered carefully.

The single collector contact efficiency ($\eta_o$) established by Yao *et al.* [38] as a ratio comparing the rate at which particles encounter a collector to the rate at which they flow towards the collector, combines the three mechanisms of sedimentation, interception and brownian diffusion into a single term:

$$\eta_o = \eta_G + \eta_I + \eta_D \tag{2.10}$$

Calculations are based on the approach by Tufenkji & Elimelech [62] who further refined the single collector contact efficiency to account for hydrodynamic interactions and van der Waals forces.

However, the single collector contact efficiency ($\eta_o$) does not consider electrostatic forces (repulsion), because they are assumed to be negligible under favorable deposition conditions. In order to capture particle retention under unfavorable deposition conditions with repulsive interactions between colloids and collector, the concept of attachment efficiency ($\alpha$) has been introduced to the CFT [16, 40, 62]. The attachment efficiency represents the fraction of collisions between suspended particles and collector grains that results in attachment (entrapment in the secondary minimum). As demonstrated by Yao *et al.* [38] it can be determined empirically from column experiments, using the normalized concentration ($C/C_o$) at the stable plateau of the breakthrough curves:

$$\alpha = -\frac{2d_c}{3(1-n)\eta_o L}\ln(\frac{C}{C_o}) \tag{2.11}$$

where $d_c$ is the average diameter of the collector. Average mean diameters obtained

Table 2.3.: Parameter values assumed for calculation of the single collector contact efficiency using the approach by Tufenkji & Elimelech [62].

| **Parameter** | **Symbol** | **Value** | **Unit** |
|---|---|---|---|
| Hamaker constant [a] | A | $9.30e^{-20}$ | kg m$^{-2}$ s$^{-2}$ |
| Particle density [b] | $\rho_p$ | 1145 | kg m$^{-3}$ |
| Fluid density | $\rho_f$ | 1000 | kg m$^{-3}$ |
| Fluid viscosity | $\mu_f$ | 0.001 | kg m$^{-1}$ s$^{-1}$ |

[a]Hamaker constant was taken from Lince *et al.* [63] and [b]particle density was assumed to be equal the PCL density stated by Sigmar Aldrich.

by Dynamic Light Scattering (Figure 3.2), were used for all calculations regarding the colloid filtration theory, neglecting larger particle aggregates detectable by other techniques (Eyetech). For equation 2.11 to be valid, advection has to be the dominant mechanism of nanoparticle transport in the packed column experiments. This is usually the case for most laboratory column experiments, but can be violated under conditions of extremely low approach velocities where dispersion becomes dominant [16]. The rate at which colloids are deposited onto the collector surface under unfavorable deposition conditions can then be calculated with the following equation:

$$k_{\mathrm{dep}} = \frac{3(1-n)}{2d_{\mathrm{c}}} v \alpha \eta_{\mathrm{o}} \tag{2.12}$$

with $k_{\mathrm{dep}}$ as deposition rate coefficient.

## 2.6. Statistical analysis

R (version 3.1.0) by R Core Team [64] was used for statistical analysis. For analysis of variance (ANOVA) the aov-function was applied. Normal distribution was tested with Shaprio and homogeneity of variances by Bartlett, both functions of the ”stats” package. In case of unequal variances a Welch-test was conducted. Post-hoc tests for pairwise comparisons were done by computing the ”Tukey Honest Significant Differences” with the TukeyHSD-function or applying a pairwise t-test with Bonferroni correction in case of unequal variance.

# 3. Results and discussion

## 3.1. Nanoparticle characterization

The Zetasizer measurements were significantly different for all three suspensions ($F_{(2,12)} = 1129, p = 2.19e^{-14}$) and their pairwise comparisons (Figure 3.1).

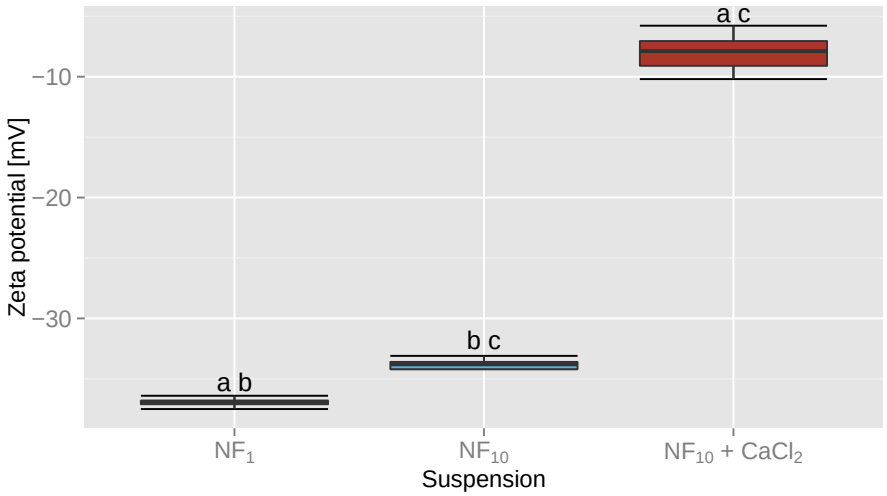


Figure 3.1.: Zeta potential of the nanoparticles in $NF_1$, $NF_{10}$ and $NF_{10}$+$CaCl_2$. The central solid line marks the median, boxes the 1st and 3rd quartile and whiskers the greatest value measured for each suspension. **(a - c)** denote significant differences in zeta potential between suspensions based on multiple comparison. **(a)** $p \leq 0.001$, **(b)** $p = 0.0013$, **(c)** $p \leq 0.001$.

The particle size distribution obtained by the Dynamic Light Scattering measurements can be described by two values (Figure 3.2), a mean value for the hydrodynamic diameter (Z-Average) and a width parameter known as Polydispersity Index (PDI). The PDI is a measure of particle size heterogeneity in mixtures, with a small value ($\sim$0.2) indicating a rather uniformly, monodispersed particle suspension. Statistical analysis revealed an overall significant difference in means ($F_{(2,7.6)} = 12.49, p = 0.004$) and PDI ($F_{(2,12)} = 23.46, p \leq 0.001$) of the particle size distribution.

Eyetech measurements, which reveal the presents of larger particles ($\geq$1 µm) in suspension, were used for a more conclusive insight into the particle size distribution.

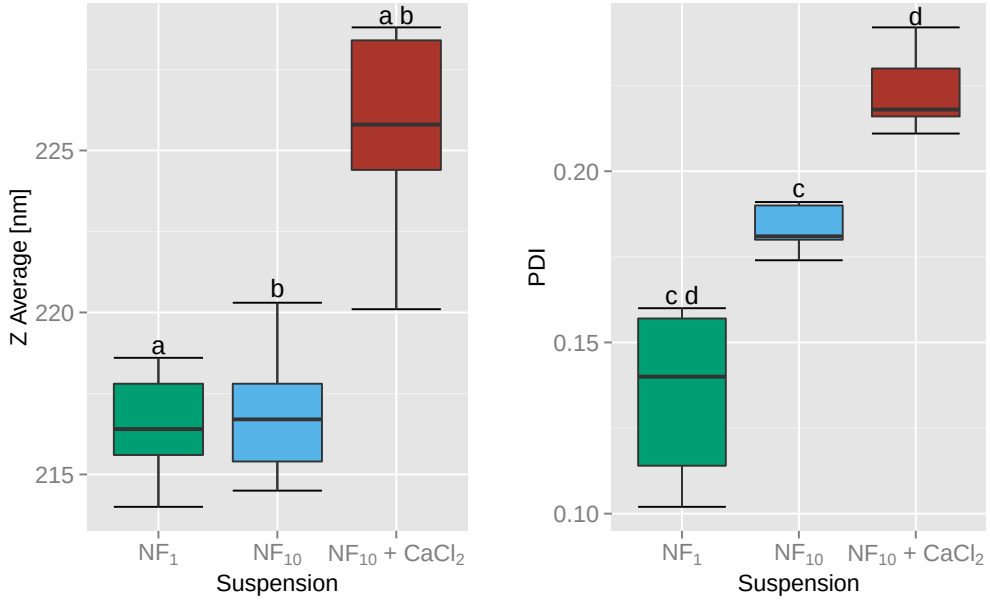


Figure 3.2.: Particle size distributions of the nanoparticles in suspension characterized by mean size (Z-Average) and PDI. The letters **(a - d)** indicate a significant difference in Z-average and PDI between two suspensions with **(a)** $p = 0.0068$, **(b)** $p = 0.0083$, **(c)** $p = 0.0032$, **(d)** $p = 0.0001$ .

The Eyetech number based size distributions in Figure 3.3 indicate rather high uniformity in mean particle size across all three suspension for 90 % of the particles (D90 = 3.92 µm to 6.42 µm). However, the upper 10 % of particles in each sample is substantially larger with a maximum size between 16.78 µm and 34.66 µm (Table 3.1). The volume based size distributions yield similar results, but suggest a more even distribution of particle sizes for each suspension with an overall strong tendency towards larger diameters (mean = 7.62 µm to 16.92 µm).

Overall, measurements with Dynamic Light Scattering and Eyetech indicate

Table 3.1.: Particle size distribution statistics of the nanoparticles in suspensions obtained by EyeTech measurements.

| | **Number** | | | **Volume** | | |
|---|---|---|---|---|---|---|
| | mean ± SD | D90 | max | mean ± SD | D90 | max |
| $NF_1$ | 3.04 ±3.00 | 6.42 | 29.48 | 16.92 ±9.17 | 28.85 | 29.48 |
| $NF_{10}$ | 3.07 ±2.39 | 5.49 | 34.66 | 13.86 ±8.56 | 26.98 | 34.66 |
| $NF_{10}$+$CaCl_2$ | 2.08 ±1.61 | 3.92 | 16.78 | 7.62 ±4.33 | 14.43 | 16.78 |

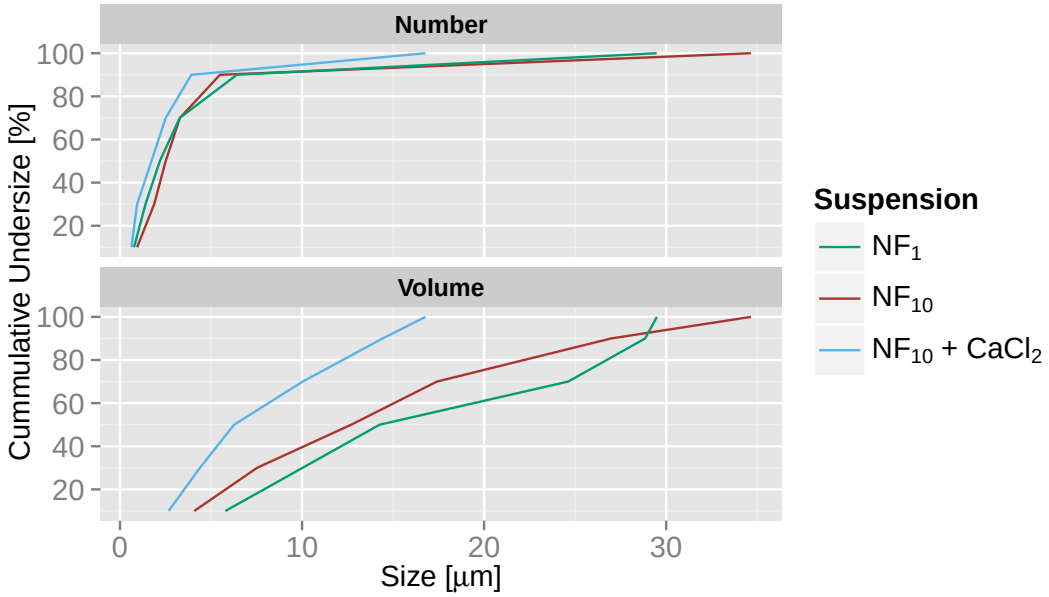


Figure 3.3.: Particle size distributions of the larger nanoparticle size fraction for all suspensions. Results are plotted as minimal cumulative distribution functions of the mean size of the particles. Mean size was both calculated by a weighted number as well as a weighted volume based function and presented in two separate graphs.

that particle size distributions are not monodispersed. They rather consist of a stable size fraction of small particles of around 220 nm and a fraction of larger aggregates ranging up to several micrometers in size. This leads to the conclusion, that the nanopesticide particles are less stable in suspension than previously expected, because even the supposedly stable suspension $NF_1$ showed strong signs of aggregation less than 1 hour after preparation as indicated by the EyeTech results (Figure 3.3).

### 3.1.1. Effect of increased particle concentration

An increased nanoparticle concentration between $NF_1$ and $NF_{10}$ was originally not expected to significantly influence zeta potential. Previous studies observed a dependency of zeta potential and particle concentration [52, 65, 66] for very dilute solution of, for example, purified water. However, the significant difference in zeta potential between $-36.94 \pm 0.40$ mV ($NF_1$) and $-33.78 \pm 0.46$ mV ($NF_{10}$) can probably be attributed to heterogeneities in PCL polymer structure and configuration [68].

It has to be noted that repeated measurements are not completely independent, but have been taken from the same suspension sample over a period of time, emphasising the possibility of simple heterogeneity in suspension being responsible for

an observed statistically significant difference between $NF_1$ and $NF_{10}$ ($p = 0.0013$).

Nevertheless, in terms of particle transport and deposition behavior, a drop in zeta potential by 3.16 mV with increased particle concentration seems negligible, because the overall potential stays negative.

Increase in particle concentration did not have a significant effect on mean particle size ($216.48 \pm 1.81$ nm ($NF_1$), $216.94 \pm 2.26$ nm ($NF_{10}$)). With $0.13 \pm 0.03$ ($NF_1$) and $0.18 \pm 0.01$ ($NF_{10}$) the PDI was statistically significantly different, but rather low and still hinting at a monodispersed particle suspension. Therefore, a relevant effect on transport and particle deposition behavior due to increased nanoparticle concentration can be ruled out.

### 3.1.2. Effect of increased ionic strength

Addition of the electrolyte $CaCl_2$ to the nanoparticle suspension caused a pronounced and significant drop in zeta potential towards a more positive value of $-8.00 \pm 1.73$ mV ($NF_{10}$+$CaCl_2$). This is in accordance to the DLVO theory, where the actual zeta potential of the particles drops with increasing ionic strength [24]. At high ionic strength the diffuse layer around the particles is compressed (*Double-layer compression*) and the Stern layer potential decreases. The zeta potential, measured at the shear plane, can be seen as a practical approximation of the potential at the stern layer [24].

Furthermore, the *Double-layer compression* encompasses a shorter range of repulsive forces (charge screening) [24]. As a result, the close approach of particles due to Van der Waals forces is much more likely. Therefore, addition of $CaCl_2$, an electrolyte with divalent cations, is expected to cause substantial aggregation [34].

The actual increase in particle size ($225.50 \pm 3.53$ nm) and PDI ($0.22 \pm 0.01$) that was observed through Dynamic Light Scattering was rather small, considering the anticipated induced aggregation of particles. On the contrary, Eyetech measurements even suggest a drop in mean and maximum particle size (Table 3.1).

However, it has to be noted that an immediate increase in turbidity and deposition of visible particles onto the flask wall was detectable upon addition of $CaCl_2$. It is highly likely that these were not measurable by analyzing the laser obscuration time (Eyetech). The existence of an additional fraction of extremely large particles in suspension, which immediately deposited onto the flask walls could help to explain the unexpected measured drop in aggregate size with increased ionic strength. Most particles of the previously large size fraction would have aggregated even further and deposited onto the flask wall, only leaving behind a relatively stable fraction of much smaller particles still afloat in suspension. Therefore, particle destabilization through increased ionic strength was sucessful, but not directly recognisable from the measurement results. To prevent deposition and settling of aggregates onto the flask walls during the injection phase of the column experiments, all suspensions were constantly stirred.

## 3.2. Porous media characterization

Streaming potentials determined for pure glass beads and a solution containing 1 mmol NaCl revealed an extremely high, negative zeta potential ($-104.6 \pm 3.8$ mV) across the full pH range investigated (Figure 3.4). Similar results have been reported by previous studies on zeta potentials of glass surfaces in aqueous solutions [69, 70]. Equivalent conditions are expected during column experiments with a solution of the pure active ingredient atrazine in 0.1 % ACN (*Exp-Atr*, pH = 5.95) and the suspension $NF_1$ (pH = 4.43).

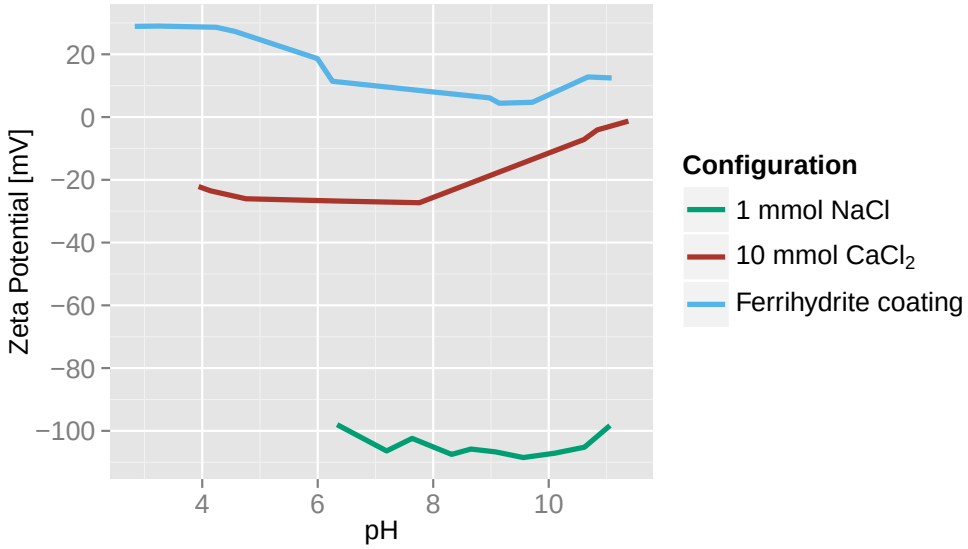


Figure 3.4.: Zeta potential (mV) of porous media as a function of pH for all relevant configurations used during the column experiments.

A relatively less negative zeta potential was found for a solution containing 10 mmol $CaCl_2$ ($-17.3 \pm 11.1$ mV), representing column experiment conditions where a solution of $NF_{10}$+$CaCl_2$ (pH = 4.42) is employed. As expected, with addition of the electrolyte $CaCl_2$, the zeta potential at the glass bead surface - water interfaces is lower due to the already described process of *Double-layer compression* at higher ionic strength [24].

Measurements conducted with ferrihydrite coated glass beads and a 10 mmol $CaCl_2$ solution resulted in an overall small, net positive potential of the collector surface ($16.8 \pm 10.1$ mV). The technique had already been successfully employed in previous studies for the coating of quartz sand [71, 72]. Iron oxide coating successfully changed the surface charge distribution of the collector surface (glass beads), resulting in a higher number of positively charged surface sites.

## 3.3. Column experiments

Four separate sets of column experiments were conducted to investigate the effect of a) encapsulation, b) ionic strength and c) heterogeneous surface charge of the collector on transport and deposition behavior. Table 3.2 gives an overview on variation in experimental conditions across all experimental settings.

The total atrazine concentration of each sample collected was measured and quantified via HPLC and compared to breakthrough curves (BTC) of the ideal tracer $NaNO_3$ (Figure 3.5 and 3.6).

The nanocapsules are known to experience 50 % release of the AI within 1.2 days of preparation [1]. Consequently, solute and colloidal transport are both present and cannot clearly be distinguished by measuring total atrazine concentrations. However, total atrazine concentration measured at the column outlet might still serve as a rough proxy for encapsulated (colloidal) AI transport, because atrazine in solution is expected to pass through the columns unhindered.

Table 3.2.: Overall characterization of the column experiments.

| | **Porous Media** | | **Suspension** | | | | |
|---|---|---|---|---|---|---|---|
| **Experiment** | **beads** | $\phi_{\mathbf{Zeta}}$* mV | **$CaCl_2$** mmol $L^{-1}$ | **NF** mg $L^{-1}$ | **AI** mg $L^{-1}$ | **pH** | $\phi_{\mathbf{Zeta}}$ mV |
| Exp-Atr | uncoated | -98.02 | 0 | 0 | 1 | 5.95 | -36.94 |
| Exp-NF | uncoated | -98.02 | 0 | 1.25 | 1.14 | 4.35 | -33.78 |
| Exp-$NF_{CaCl_2}$ | uncoated | -23.50 | 10 | 10 | 9.66 | 4.42 | -8.00 |
| Exp-$NF_{Iron}$ | coated | 27.28 | 10 | 10 | 9.40 | 4.42 | -8.00 |

*value of the closest streaming potential measurement point of the electrokinetic analyser in regard to pH of each suspension.

Initial breakthrough time of the various particle suspensions was similar to that of the tracer, with a rise and steady increase in $C/C_0$ at around 1 PV. All breakthrough curves reached a plateau at approximately 1.3 to 1.5 PV.

A mass balance based on effluent and influent concentrations of atrazine reveals complete recovery of the AI for all conducted column experiments ($rec_{AI} = 1.00$).

### 3.3.1. Influence of AI encapsulation

Encapsulation of the AI had no visible effect on transport and deposition (Figure 3.5 a and b). Uncoated glass beads with a strong negative surface potential (−98.02 mV, Table 3.2) were used in both, *Exp-Atr* and *Exp-NF*. This resulted in unfavorable deposition conditions in case of *Exp-NF*. Particle breakthrough

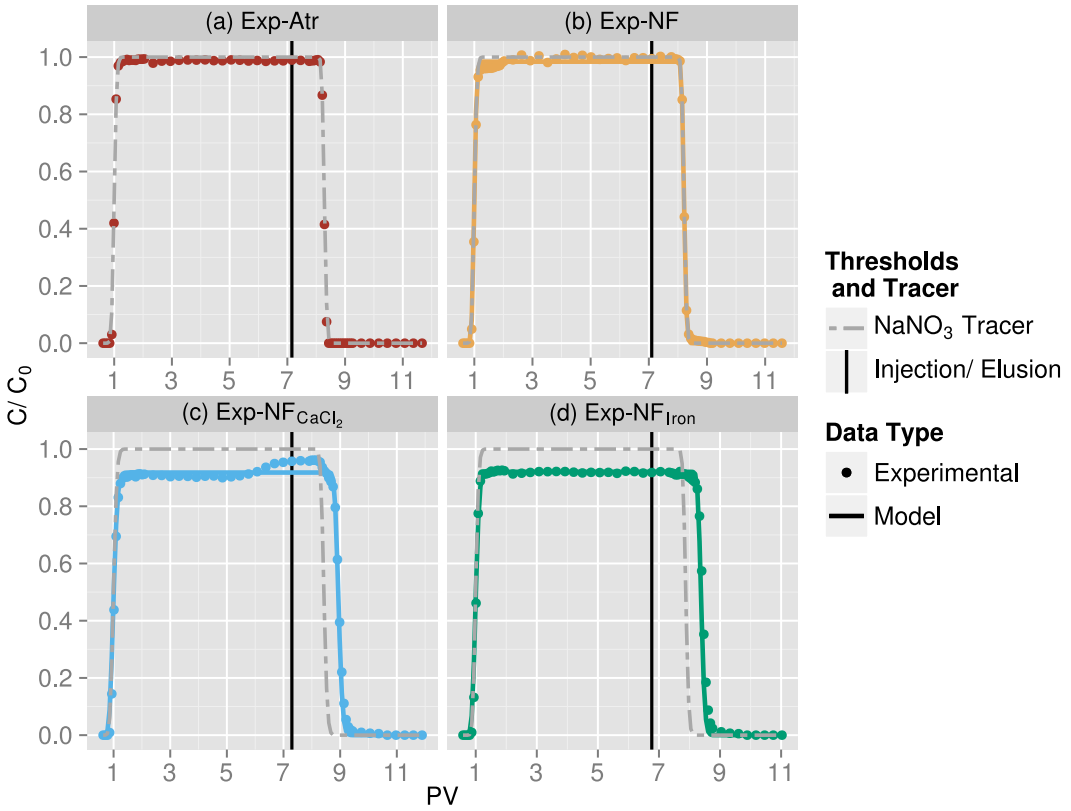


Figure 3.5.: Breakthrough curves as a function of pore volume. Dots represent measurements while lines are model fits (solid and dashed, for atrazine and tracer, respectively). Straight vertical lines mark the switch between injection and elusion phase.

reached a plateau at a relative average concentration $C/C_0$ of 1.00 (atrazine) and 0.99 (NF), respectively.

Overall, transport of the pure AI and also encapsulated in the nanocarrier was identical to that of the conservative tracer $NaNO_3$. This indicates that neither sorption of the AI nor attractive interactions between nanopesticide (PCL polymers) and collector caused any retention. Furthermore, physical properties of the nanopesticide (e.g, larger size) did not affect AI transport.

### 3.3.2. Influence of increased ionic strength

$CaCl_2$ was used as an electrolyte in order to determine the effect of increased ionic strength on transport and deposition of the nanopesticide. The $NF_{10}$+$CaCl_2$ suspension was injected into columns packed with uncoated glass beads (*Exp-*$NF_{CaCl_2}$, Table 3.2).

The nanoparticle suspension breakthrough curve *Exp-*$NF_{CaCl_2}$ leveled out at a

plateau concentration of around 0.92 (Figure 3.5 c). This suggests that a fraction of the nanopesticide was retained due to the previously mentioned changes in particle characteristics (e.g., zeta potential, large aggregates) upon increased ionic strength.

### Retention in flow stagnation zones

Reduced repulsive interactions through lowering of the energy barrier between particle and collector (*Double-layer compression*) [16] increase the likelyhood of successful collisions. However, the atrazine containing nanocapsules as well as the glass beads both express a net negative charge, which likely still yields an energy barrier to attachment, preventing irreversible attachment in the primary energy minimum [29]. Reversible retention in a weak secondary energy minimum is more likely to occure.

Colloids associated with the collector surface by a secondary energy minimum, are retained without direct contact to the surface and are subject to hyrodynamic drag forces [46]. Although, the rather low, applied injection velocity ($3.44 \times 10^{-6}\,\mathrm{m\,s^{-1}}$) only leads to comparably weak dragging forces, it does promote a large volume of stagnation zones [57]. Stagnation zones are locations of zero flow velocity within the porous media and have recently been demonstrated to induce retention for colloid to collector ratios of less than about 0.005, with this number increasing as flow velocity decreases [29, 46]. Flow stagnation zones are expected to be the ultimate locations of retention for secondary minimum associated particles, as they diffuse along the grain surface into these zones [46].

Furthermore, colloid - colloid interactions might actually limit the maximum number of particles being retained in the stagnation zone volume available [46]. The occurrence of a second rise in relative concentration $C/C_0$ of the BTC to a plateau of 0.96 (PV $\sim$5.5) could be interpreted as the result of retention site saturation within those flow stagnation zones.

### Straining

Earlier size measurements and visual observations (Section 3.1) confirm the presence of large particle aggregates in suspension ($\geq$1 µm). The calculated ratio of particle to collector diameter ($\geq$0.005, Section 2.5.2) is theoretically large enough for straining in dead-end pores to occure (Figure 2.7) [29, 46]. The slightly lower effluent total atrazine concentrations ($C/C_0$ = 0.92) could therefore be explained by straining of AI containing nanocapsule-aggregates. The second rise in relative concentration could also be interpreted as the result of all available dead-end pores being blocked.

Effluent concentrations (*Exp-NF*$_{CaCl_2}$) rapidly decrease back to $C/C_0 = 0$ after setting in of the elusion phase, following the trajectory of the tracer BTC. Therefore,

detachment and re-entrainment is probably caused by a rapid change in physiochemical conditions. Increased pH, a drop in ionic strength due to the absence of the tracer or a temporary change in flow velocity [73] should be considered. High colloidal detachment rates usually cause a visible tailing of the BTC [29], which is not the case here. Additionally, strained particles are generally not re-entrained to a large extent [29]. Nevertheless, strained particles can be partially remobilized upon changes in hydrodynamic conditions (e.g., flow reversal, approach velocity) and solution chemistry (e.g., ionic strength) [39].

Overall, both retention mechanisms explain the increase in particle deposition during the injection phase, but neither one fully captures the observed rapid and complete re-entrainment of the nanopesticide ($rec_{\mathrm{AI}} = 1.00$) during the elusion phase. Nevertheless, the increase in ionic strength clearly affects the AI transport behaviour.

### 3.3.3. Influence of collector surface charge heterogeneity

The $NF_{10}$+$CaCl_2$ suspension was injected into a column packed with ferrihydrite coated glass beads (*Exp-*$NF_{Iron}$). The experimental conditions comprised heterogeneous and net positive surface charge of the collector ($\phi_{\mathrm{Zeta}} = 27.28\,\mathrm{mV}$) as well as high ionic strength (Table 3.2). The BTC does not show any additional nanopesticide retention when compared to *Exp-*$NF_{CaCl_2}$ ($C/C_0 = 0.92$, Figure 3.5 d). The anticipated local absence or reduction of an energy barrier to attachment through surface charge heterogeneity was either too insignificant to have an additional effect on deposition of the nanoparticles, or the previous assumption of particles being retained in a secondary energy minimum was not applicable in the first place.

With breakthrough curves plotted against time instead of pore volume (Figure 3.6), differences in porosity and flow rate are neclected. Apparently, increased surface charge heterogeneity had no additional effect on the overall plateau concentration ($C/C_0$) and general shape of the BTC when compared to *Exp-*$NF_{CaCl_2}$. The absence of a second plateau and rise in relative concentration (at PV $\sim$5.5) in comparison to *Exp-*$NF_{CaCl_2}$ (Figure 3.5 c) is the only clear indication of surface charge heterogeneity affecting transport and deposition behaviour.

Overall, electrostatic interactions did not immidiately result in higher particle deposition rates through attachment, but they somehow affected long-term retention of the AI within the porous media, apparent in the absence of a second rise in relative concentration.

### 3.3.4. Transport models and filtration theory

In general, the leveling out of all breakthrough curves, reaching a relative concentration plateau at 1.3 to 1.5 PV independent of particle suspension and porous

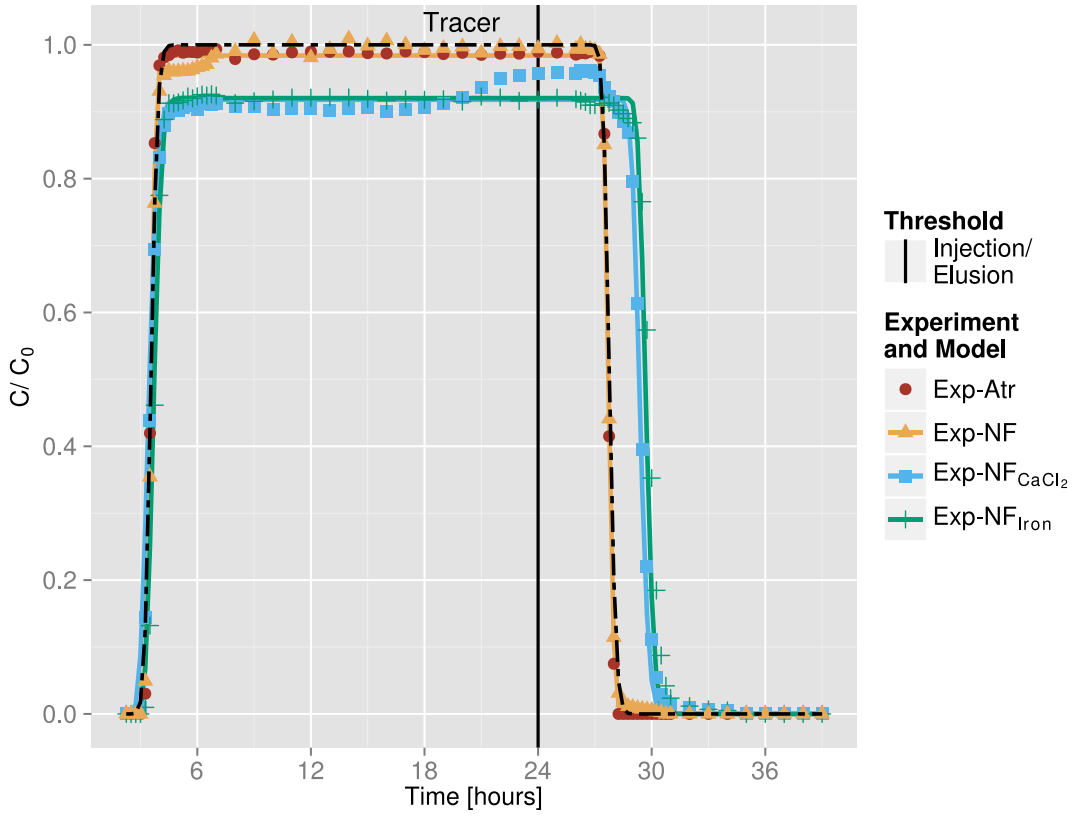


Figure 3.6.: Breakthrough curves of all conducted experiments as a function of time. Point data represents actual measured experimental relative sample concentrations whereas the corresponding solid lines were fitted using the CDE implemented in STANMOD. The straight vertical line marks the switch between injection and elusion phase.

media indicates that the active ingredient atrazine and supposedly the encapsulating nanocarriers are removed at a constant rate [57]. With the aim to apply colloidal filtration theory, which requires steady-state effluent conditions [76], a number of simplifications were made. These included omission of the second rise in relative concentration for $Exp\text{-}NF_{CaCl_2}$. Further simplifications (e.g., neglecting the effect of straining, blocking or detachment on particle transport) had to be accepted in order to use a simple convection-dispersion equation with a single coefficient for irreversible first-order particle removal ($k_{rem}$) [77].

The CDE (equation 2.3) fitted the data very well in all cases ($r^2 \geq 0.988$), which confirms that deposition can generally be described by first-order kinetics. The removal rate coefficient value ($k_{rem}$) was as low as $5.38 \times 10^{-7}$ (*Exp-NF*) and increased by about one order of magnitude to $2.80 \times 10^{-6}$ ($Exp\text{-}NF_{Iron}$) and $2.95 \times 10^{-6}$ ($Exp\text{-}NF_{CaCl_2}$). The hydrodynamic dispersion coefficient (D) was not zero, but ranges from 0.000 71 to 0.002 10 (Table 3.4), which most likely can be attributed to the rather low flow velocity ($v_f \approx 3.4 \times 10^{-6}$).

Table 3.4.: Summary of all parameters obtained by fitting the convection-dispersion equation (CDE) to the experimental breakthrough curves as well as all relevant input parameters.

| **Experiment** | $\mathbf{d_c}$ nm | **n** | $\mathbf{v_f}$ m $s^{-1}$ | **D** $cm^2$ $s^{-1}$ | $\mathbf{r^2}$ | $\mathbf{k_{rem}}$ $s^{-1}$ | $\boldsymbol{\alpha_{CDE}}$ |
|---|---|---|---|---|---|---|---|
| Exp-NF | 216.9 | 0.40 | $3.34e^{-6}$ | 0.00071 | 0.999 | $5.38e^{-7}$ | 0.00014 |
| Exp-$NF_{CaCl_2}$ | 225.5 | 0.40 | $3.44e^{-6}$ | 0.00210 | 0.993 | $2.95e^{-6}$ | 0.00079 |
| Exp-$NF_{Iron}$ | 225.5 | 0.43 | $3.38e^{-6}$ | 0.00148 | 0.988 | $2.80e^{-6}$ | 0.00083 |

Mean diameter of the collector ($d_c$), porosity (n), flow velocity ($v_f$), hydrodynamic dispersion coefficient (D), coefficient of determination ($r^2$), removal rate coefficient ($k_{rem}$) and attachment efficiency ($\alpha_{CDE}$).

The similarity between deposition rate coefficients ($k_{dep}$) and the corresponding removal rate coefficient ($k_{prm}$) as well as between the attachment efficiencies ($\alpha_{CFT}$) and ($\alpha_{CDE}$) supports that advection and not dispersion is the dominant transport mechanism [57]. The CFT and CDE based attachment efficiencies ranged from 0.000 14 to 0.000 83 (Table 3.6) and from 0.000 06 to 0.000 83 (Table 3.4), respectively. Therefore, both approaches, CFT and CDE, are suitable to evaluate deposition kinetics and transport behaviour of the nanoparticle in suspensions used in this study.

The CFT incorporates diffusion, interception and gravitational sedimentation (Figure 2.7) as modes of particle transport from the fluid to the grain surface (collector) in order to explain and quantify particle deposition [26, 28, 38].Figure 3.7 graphically represents the relevant transport mechanisms accounted for by CFT. The single-collector contact efficiency ($\eta_o$) can be calculated using CFT [62], which was nearly the same for all conducted column experiments with $\eta_o$ values ranging from 0.234 to 0.256 (Table 3.6) for an assumed average particle size ($d_c$) of ∼220 nm (Table 3.4). All colloidal filtration theory calculations are based on the assumptions, that the relatively monodispersed size fraction of small particles (∼220 nm in

Table 3.6.: Summary of all transport and deposition parameters obtained from CFT calculations.

| **Experiment** | $\boldsymbol{\eta_D}$ | $\boldsymbol{\eta_I}$ | $\boldsymbol{\eta_G}$ | $\boldsymbol{\eta_o}$ | $\boldsymbol{\alpha_{CFT}}$ | $\mathbf{k_{dep}}$ $s^{-1}$ |
|---|---|---|---|---|---|---|
| Exp-NF | 0.25514 | 0.00037 | 0.00070 | 0.25621 | 0.00006 | $2.47e^{-7}$ |
| Exp-$NF_{CaCl_2}$ | 0.24111 | 0.00039 | 0.00073 | 0.24223 | 0.00081 | $3.03e^{-6}$ |
| Exp-$NF_{Iron}$ | 0.23328 | 0.00034 | 0.00075 | 0.23437 | 0.00083 | $2.82e^{-6}$ |

Share of diffusion ($\eta_D$), interception ($\eta_I$) and gravitational sedimentation ($\eta_G$) in single-collector contact efficiency ($\eta_o$), the resulting attachment efficiency ($\alpha_{CFT}$) and deposition rate coefficient ($k_{dep}$).

mean size) prevails in terms of absolute particle numbers in suspension (Table 3.4) and can be used as a proxy for the general particle size distribution. Diffusion ($\eta_D \approx 0.23$ to 0.26) was by far the dominant transport mechanism from the fluid to the collector (Table 3.6) for this particle size fraction. Sedimentation becomes the major mechanism only for particles larger than 2 µm. However, the existence of a substantial fraction of larger particles in volume and number would also favor straining as a dominant process for particle removal, with the ratio of particle to collector diameter being larger than 0.005 [29].

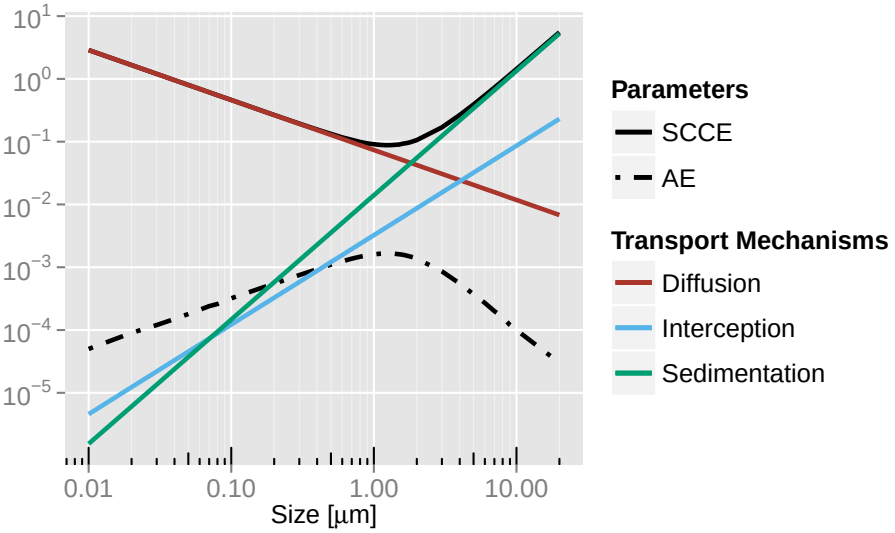


Figure 3.7.: Graphical representation of the CFT transport mechansims: (**a**) diffusion, (**b**) interception and (**c**) gravitational sedimentation in single-collector contact efficiency (SCCE, $\eta_o$) and the related change in attachment efficiency (AE, $\alpha_{CFT}$). Values are calculated based on *Exp-NF*$_{CaCl_2}$.

According to Laumann *et al.* [57] a high similarity in $\eta_o$ is to be expected, because input parameters used for calculations (e.g., porosity, temperature, mean collector diameter, particle density, flow velocity, and fluid viscosity) were nearly identical. The moderate single-collector contact efficiencies in combination with low attachment efficiencies also support the earlier stated assumption, that attachment conditions are largely unfavorable and repulsive forces prevail, because most particle approaches do not result in attachment to the collector surface. Although, based on the $\eta_o$ values, conditions generally seem to favor encounters of particles and grain surfaces (glass beads). The rise in particle deposition through higher ionic strength is reflected in an increase of the particle deposition rate ($k_{dep}$) by about one order of magnitude from $2.47 \times 10^{-7}$ (*Exp-NF*) to $3.03 \times 10^{-6}$ (*Exp-NF*$_{CaCl_2}$), as well as the particle removal rate ($k_{dep}$) calculated via CDE (Table 3.4). In congruence with the BTC results, $k_{dep}$ did not accelerate further ($2.82 \times 10^{-6}$) upon additional increase in surface charge heterogeneity.

### 3.3.5. Release rates

Previous experiments on the release of atrazine from the PCL nanocarrier suggest a two step release: a rapid release of 50 % of the AI within 1.2 days followed by a slow release phase over an extended period of time [33]. The first phase is thought to be driven mainly by the relaxation of the polymer chains [1]. A conducted experiment (Figure 3.8), measuring the release rate of the AI from the PCL polymer, did not agree with this release profile. The employed filter device allowed for unhindered passage of atrazine in solution, which means that most of the active ingredient injected into the device, was recovered after filtration ($C/C_o = 0.96 \pm 0.01$). There was no significant difference in release ($F_{(2,2)} = 7.786, p = 0.0686$) between pure AI and the nanoparticle suspension ($0.95 \pm 0.07$ ($NF_1$)). However, the $NF_{10}$+$CaCl_2$ suspension seems to express a slight tendency towards lower release rates ($0.85 \pm 0.04$).

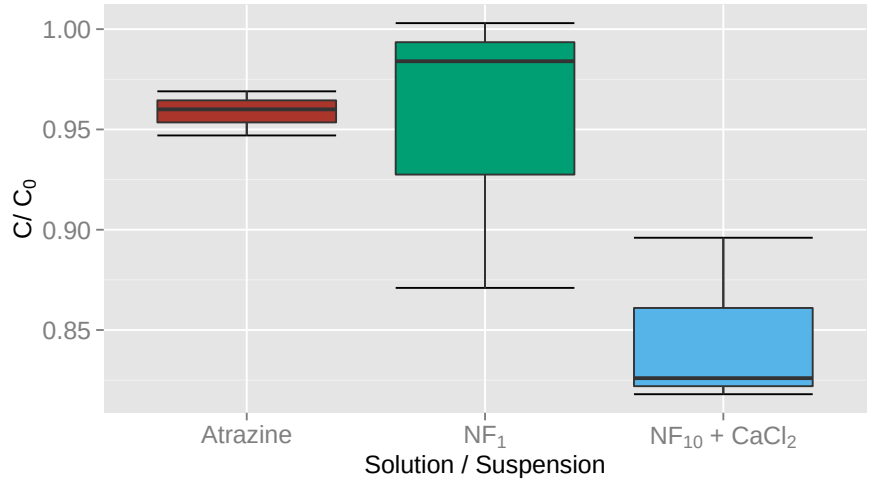


Figure 3.8.: Relative atrazine concentration ($C/C_o$) for a filtered pure atrazine solution and two filtered nanoformulation suspensions ($NF_1$ and $NF_{10}$+$CaCl_2$) approximately one hour after sample preparation.

Apparently, first phase release happened much faster than would have been expected. The results indicate that most atrazine is in solution after one hour of sample preparation and passes through the column unaffected by colloidal properties. Dilution of the stock suspension probably provoked the rapid release of atrazine and explains the discrepancies with results reported by Grillo *et al.* [1]. A lower dilution factor for *Exp-*$NF_{CaCl_2}$ could be the reason why release rates were not quite as high, one hour after sample preparation.

Overall, atrazine transport was probably less affected by colloidal properties than previously assumed. In principle, three different scenarios need to be considered (Figure 3.9): a) complete encapsulation of the AI and displacement governed

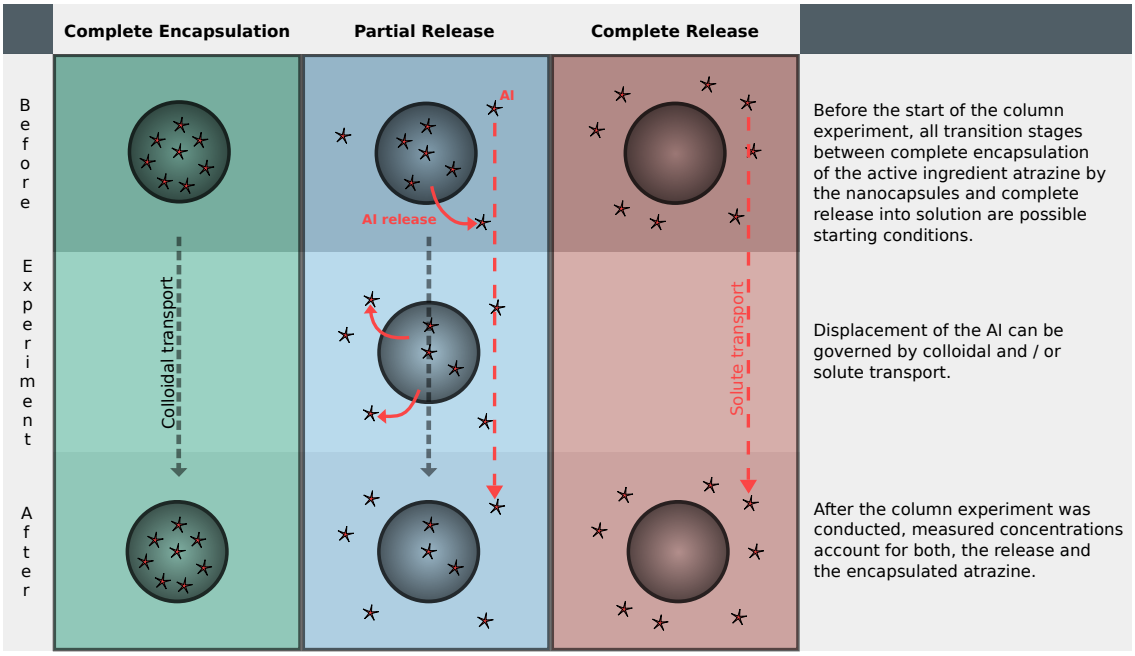


Figure 3.9.: Three transport and displacement scenarios for the active ingredient (AI) during the column experiments, incorporating encapsulation and release.

by colloidal transport, b) partial release of the AI before and during the column experiment, with solute transport taking place and, c) complete release of the AI. Scenario (b) describes the situation at hand, with displacement happening to a large extent through solute transport. Considering this, a 8 % drop in relative concentration (BTC) upon addition of $CaCl_2$ could represent the retention of most of the atrazine still being encapsulated (Figure 3.8). The remaining 92 % AI is primarily being displaced by solute transport. With aggregation taking place, sedimentation and straining are the dominant mechanisms of particle removal in this scenario. This would also explain, why increased surface charge heterogeneity had no additional effect on the overall deposition rates. All of the AI that remains encapsulated after dilution is already captured in (temporarily) stable nanoparticle aggregates physically retained by the porous media. Accordingly, the second rise in relative concentration observed after approximately 18 h for the BTC of $Exp\text{-}NF_{CaCl_2}$ BTC (Figure 3.6) can be interpreted as slow release of the AI from the retained (strained) nanoparticles instead of a saturation of available retention sites in flow stagnation zones or limitation of dead-end pores for straining. The absence of a second rise in $C/C_0$ during $Exp\text{-}NF_{Iron}$ suggests that the changed surface conditions of the collector somehow prevented further release of the AI from the polymers. With the onset of the elusion phase all of the trapped nanocarrier aggregates were either completely destabilized, detached or the AI completely released.

# 4. Conclusion

The results of this study show that the provided nanopesticide formulation is polydispersed upon dilution with clear signs of aggregation, independent of the ionic strength. The measured mean aggregate size varied between 2 and 3 µm for all suspensions, with substantially larger visible particles accumulating on the flask walls for increased ionic strength. All suspensions also contained a stable size fraction of small particles with a narrow size distribution around 220 nm.

Initial release rates of the active ingredient (AI) proved to be very high, with 85 % to 96 % of all atrazine being in solution, less than one hour after sample preparation. Therefore, the measured release rates on the diluted formulation was much higher than previously reported for the pure formulation [1]. Consequently, solute transport of the AI prevails and only a small fraction of the AI is subject to collodial transport and deposition behavior in the porous media. This also explains, why encapsulation of the AI showed no effect.

The addition of the electrolyte $CaCl_2$ on the other hand did increase retention of the nanopesticide, despite high release rates. A tendency towards slightly lower release rates was observed for increased ionic strength (85 % release). The CDE based transport model and CFT both confirmed an increase in attachment efficiency and deposition rate for the stable particle size fraction by approximately one order of magnitude upon increased ionic strength. The transport model was simplfied (eg., no straining or detachment parameter), but very good fits were observed, which suggests that removal is indeed governed by first-order kinetics. Overall, straining and sedimentation are the likely deposition mechanisms based on the polydispersed size distribution and the observed size fraction of large particles.

Furthermore, the introduced surface charge heterogeneities through ferrihydrite coating of the glass beads (collector) did affect the long-term AI deposition and transport behaviour. It either prevented re-entrainment of the nanopesticide or the AI release from the retained nanocapsules, because the BTC ($Exp\text{-}NF_{Iron}$) showes no second rise in relative concentration ($C/C_o$). Overall, the BTC confirmed first-order kinetics for the removal of the AI, but did not indicate an affect on the overall measured relative concentrations. Subsequent investigations should focus on highly concentrated suspensions with slower release profiles in order to identify possible additional effects of surface charge heterogeneity on the nanopesticde deposition behaviour.

The calculated mass balance, showes complete recovery ($rec_{\mathrm{AI}} = 1.00$) of the influent atrazine upon dilution (elution phase) with the background solution. This

supports the assumption that the AI present in the retained nanocapsules is either completely release, or the nanopesticide remobilized. Considering this, reversible deposition due to retention in a secondary energy minimum and ultimately in flow stagnation zones is unlikely, because high colloidal detachment rates usually cause a visible tailing of the BTC [29], which is not the case here. Again, straining of the particles in dead-end pores or simple sedimentation are the likely prominant deposition mechanisms. Since straining is a strong function of distance, with most of the retention happening at the inlet of the column [29, 43], the shape of the colloidal spatial distribution within the porous media should be determined in future experiments. This would greatly help to confirm straining as a mechanism for retention of the nanopesticide atrazine.

The overall results do suggest a strong affect of the nanocarrier on transport and deposition behavior of the atrazine, especially considering the high initial release rates of the AI. Only a small portion of the AI is encapsulated and subject to colloidial transport. Therefore, an increase in ionic strength probably caused complete retention of this remaining fraction of the nanopesticide in suspension through the deposition of large aggregates. In case, the release of the AI from the nanocapsules was to be slowed down and a larger proportion of the AI remained encapsulated, physico-chemical properties (e.g., ionic strength, surface charge heterogeneity) could greatly affect the potential of groundwater leaching. It would be helpful to better quantify the individual size fractions in order to link aggregate size and distribution to the observed deposition and transport behaviour. Additionally, a direct measurement technique for the polymer particles at the column outlet could significantly facilitate data interpretation of future experiments. The nanopesticide concentrations used in this study remain limited in their application for pest controls on soils, because of the observed high release rates of the AI and particle instability upon dilution. Nevertheless, the nanopesticide showes promising characteristics that might help tackle some of the exisiting environmental issues, such as groundwater leaching, associated with atrazine applications.

# 5. Aknowledgements

First of all, I would like to thank Dr. Melanie Kah, who suggested the topic of my thesis, for her support and all the time and effort she put into supervising me along the way.

I would especially like to thank Dr. Susanne Laumann for the discussions, sharing her expertise and giving feedback and inspirations.

I also thank Prof. Dr. Thilo Hofmann for his supervision and feedback.

I am grateful to Petra Körner, Wolfgang Obermaier, Doris Schmid, Dr. Frank von der Kammer for sharing their expertise and all the very helpful advice on work in the laboratory.

Last but not least I would like to thank all those people who supported me with their good advice, their prove-reading and by editing my work.

# Bibliography


1. Grillo, R. *et al.* Poly(epsilon-caprolactone) nanocapsules as carrier systems for herbicides: physico-chemical characterization and genotoxicity evaluation. *Journal of hazardous materials* **231-232,** 1–9 (Sept. 2012).
2. Sargent Jr., J. F. *The National Nanotechnology Initiative: Overview, Reauthorization, and Appropriations Issues* tech. rep. (Congressional Research Service, 2013), 69.
3. Lauterwasser, C. *Small sizes that matter: Opportunities and risks of Nanotechnologies. Report in co-operation with the OECD International Future Programme* tech. rep. (OECD, 2005).
4. Bernhardt, E. S. *et al.* An Ecological Perspective on Nanomaterial Impacts in the Environment. *Journal of Environment Quality* **39,** 1954–1964 (2010).
5. Nel, A., Xia, T., Mädler, L. & Li, N. Toxic potential of materials at the nanolevel. *Science* **311,** 622–627 (2006).
6. Nowack, B. & Bucheli, T. D. Occurrence, behavior and effects of nanoparticles in the environment. *Environmental pollution (Barking, Essex : 1987)* **150,** 5–22 (Nov. 2007).
7. FAO/WHO [Food and Agriculture Organization of the United Nations/World Health Organization]. *FAO/WHO Paper: State of the art on the initiatives and activities relevant to risk assessment and risk management of nanotechnologies in the food and agriculture sectors* Geneva, 2013.
8. CropLife International. *Helping Farmers Grow* tech. rep. (2013).
9. Kah, M., Beulke, S., Tiede, K. & Hofmann, T. Nanopesticides: State of Knowledge, Environmental Fate, and Exposure Modeling. *Critical Reviews in Environmental Science and Technology* **43,** 1823–1867 (Jan. 2013).
10. EPA. *Pesticides Industry Sales and Usage: 2006 and 2007 Market Estimates* tech. rep. (Environmental Protection Agency, 2011), 33.
11. Coelho, S. European Pesticide Rules Promote Resistance, Researchers Warn. *Science (New York, N.Y.)* **323,** 450 (Jan. 2009).
12. Zhang, W., Jiang, F. & Ou, J. Global pesticide consumption and pollution: with China as a focus. *Proceedings of the International Academy of Ecology and Environmental Science* **1,** 125–144 (2011).

13. Elbahri, Z. & Taverdet, J. L. Optimization of an herbicide release from ethylcellulose microspheres. *Polymer Bulletin* **54,** 353–363 (May 2005).

14. Christian, P., Von der Kammer, F., Baalousha, M. & Hofmann, T. Nanoparticles: structure, properties, preparation and behaviour in environmental media. *Ecotoxicology (London, England)* **17,** 326–43 (July 2008).

15. Scientific Commitee On Emerging And Newly Identified Health Risks (SCENIHR). *Opinion on the appropriateness of existing methodologies to assess the potential risks associated with engineered and adventitious products of nanotechnologies* tech. rep. September (European Commission, 2005).

16. Petosa, A. R., Jaisi, D. P., Quevedo, I. R., Elimelech, M. & Tufenkji, N. Aggregation and deposition of engineered nanomaterials in aquatic environments: role of physicochemical interactions. *Environmental science & technology* **44,** 6532–6549 (Sept. 2010).

17. DeNovio, N. M., Saiers, J. E. & Ryan, J. N. Colloid Movement in Unsaturated Porous Media: Recent Advances and Future Directions. *Vadose Zone Journal* **3,** 338–351 (May 2004).

18. Nel, A. E. *et al.* Understanding biophysicochemical interactions at the nano-bio interface. *Nature materials* **8,** 543–57 (July 2009).

19. Sharma, A., Kawamoto, K., Moldrup, P., de Jonge, L. W. & Komatsu, T. Transport and Deposition of Variably Charged Soil Colloids in Saturated Porous Media. *Vadose Zone Journal* **10,** 1228–1241 (2011).

20. Flury, M. & Qiu, H. Modeling Colloid-Facilitated Contaminant Transport in the Vadose Zone. *Vadose Zone Journal* **7,** 682–697 (2008).

21. Woodruff, M. A. & Hutmacher, D. W. The return of a forgotten polymer—Polycaprolactone in the 21st century. *Progress in Polymer Science* **35,** 1217–1256 (Oct. 2010).

22. Sakai, H. *et al.* Preparation and properties of nanosized biodegradable polymer capsules. *Journal of oleo science* **60,** 569–73 (Jan. 2011).

23. Eisler, R. *Eisler's encyclopedia of environmentally hazardous priority chemicals* First edit (Elsevier B.V., Amsterdam, 2007).

24. Gregory, J. *Particles in water: properties and processes* (IWA Publishing, 2004).

25. Elimelech, M., Gregory, J., Jia, X. & Williams, R. A. *Particle Deposition and Aggregation: Measurement, Modelling and Simulation* (Butterworth-Heinemann, 1995).

26. Nelson, K. E. & Ginn, T. R. Colloid filtration theory and the Happel sphere-in-cell model revisited with direct numerical simulation of colloids. *Langmuir : the ACS journal of surfaces and colloids* **21,** 2173–84 (Mar. 2005).

27. Ngueleu, S. K., Grathwohl, P. & Cirpka, O. a. Effect of natural particles on the transport of lindane in saturated porous media: laboratory experiments and model-based analysis. *Journal of contaminant hydrology* **149,** 13–26 (June 2013).

28. Elimelech, M. & O'Melia, C. Effect of particle size on collision efficiency in the deposition of Brownian particles with electrostatic energy barriers. *Langmuir*, 1153–1163 (1990).

29. Bradford, S. a., Yates, S. R., Bettahar, M. & Simunek, J. Physical factors affecting the transport and fate of colloids in saturated porous media. *Water Resources Research* **38,** pages (Dec. 2002).

30. Hiemstra, T., Antelo, J., Rahnemaie, R. & Riemsdijk, W. H. V. Nanoparticles in natural systems I: The effective reactive surface area of the natural oxide fraction in field samples. *Geochimica et Cosmochimica Acta* **74,** 41–58 (Jan. 2010).

31. Zhou, D., Wang, D., Cang, L., Hao, X. & Chu, L. Transport and re-entrainment of soil colloids in saturated packed column: effects of pH and ionic strength. *Journal of Soils and Sediments* **11,** 491–503 (Jan. 2011).

32. Wang, C. *et al.* Retention and transport of silica nanoparticles in saturated porous media: effect of concentration and particle size. *Environmental science & technology* **46,** 7151–7158 (July 2012).

33. Kah, M. *et al.* Analysing the fate of nanopesticides in soil and the applicability of regulatory protocols using a polymer-based nanoformulation of atrazine. *Environmental science and pollution research international* (Jan. 2014).

34. Ottofuelling, S., Von der Kammer, F. & Hofmann, T. Commercial titanium dioxide nanoparticles in both natural and synthetic water: comprehensive multidimensional testing and prediction of aggregation behavior. *Environmental science & technology* **45,** 10045–10052 (Dec. 2011).

35. Laumann, S., Micić, V. & Hofmann, T. Mobility enhancement of nanoscale zero-valent iron in carbonate porous media through co-injection of polyelectrolytes. *Water research* **50,** 70–9 (Mar. 2014).

36. Fritz, G., Schädler, V., Willenbacher, N. & Wagner, N. Electrosteric stabilization of colloidal dispersions. *Langmuir*, 6381–6390 (2002).

37. Ryan, J. N. & Elimelech, M. Colloid mobilization and transport in groundwater. *Colloids and Surfaces A: Physicochemical and Engineering Aspects* **107,** 1–56 (Feb. 1996).

38. Yao, K., Habibian, M. & O'Melia, C. Water and waste water filtration: Concepts and applications. *Environmental science & technology* **5,** 1105–1112 (1971).

39. Bradford, S. a., Simunek, J., Bettahar, M., van Genuchten, M. T. & Yates, S. R. Significance of straining in colloid deposition: Evidence and implications. *Water Resources Research* **42,** 16 (Dec. 2006).

40. Landkamer, L. L., Harvey, R. W., Scheibe, T. D. & Ryan, J. N. Colloid transport in saturated porous media: Elimination of attachment efficiency in a new colloid transport model. *Water Resources Research* **49,** 2952–2965 (May 2013).

41. Redman, J. a., Walker, S. L. & Elimelech, M. Bacterial adhesion and transport in porous media: role of the secondary energy minimum. *Environmental science & technology* **38,** 1777–85 (Mar. 2004).

42. Xu, S., Gao, B. & Saiers, J. E. Straining of colloidal particles in saturated porous media. *Water Resources Research* **42** (Dec. 2006).

43. Bradford, S. a., Simunek, J., Bettahar, M., Van Genuchten, M. T. & Yates, S. R. Modeling colloid attachment, straining, and exclusion in saturated porous media. *Environmental science & technology* **37,** 2242–50 (May 2003).

44. Bradford, S. a. *et al.* Straining of colloids at textural interfaces. *Water Resources Research* **41** (Oct. 2005).

45. Tufenkji, N. & Elimelech, M. Breakdown of colloid filtration theory: role of the secondary energy minimum and surface charge heterogeneities. *Langmuir : the ACS journal of surfaces and colloids* **21,** 841–852 (Nov. 2005).

46. Johnson, W. P., Li, X. & Yal, G. Colloid retention in porous media: mechanistic confirmation of wedging and retention in zones of flow stagnation. *Environmental science & technology* **41,** 1279–87 (Feb. 2007).

47. Johnson, P. R., Sun, N. & Elimelech, M. Colloid Transport in Geochemically Heterogeneous Porous Media: Modeling and Measurements. *Environmental Science & Technology* **30,** 3284–3293 (Jan. 1996).

48. Bhattacharjee, S., Ryan, J. N. & Elimelech, M. Virus transport in physically and geochemically heterogeneous subsurface porous media. *Journal of contaminant hydrology* **57,** 161–87 (Aug. 2002).

49. Mudhoo, a. & Garg, V. Sorption, Transport and Transformation of Atrazine in Soils, Minerals and Composts: A Review. *Pedosphere* **21,** 11–25 (Feb. 2011).

50. Boivin, A., Cherrier, R. & Schiavon, M. A comparison of five pesticides adsorption and desorption processes in thirteen contrasting field soils. *Chemosphere* **61,** 668–76 (Nov. 2005).

51. OECD. in *OECD Guidelines for the Testing of Chemicals* January, 1–44 (OECD Publishing, 2000).

52. Kaszuba, M., Corbett, J., Watson, F. M. & Jones, A. High-concentration zeta potential measurements using light-scattering techniques. *Philosophical transactions. Series A, Mathematical, physical, and engineering sciences* **368,** 4439–4451 (Sept. 2010).

53. Cornell, R. & Schwertmann, U. *The Iron Oxides: Structure, Properties, Reactions, Occurrences and Uses* 2nd Editio, 3–527 (Wiley-VCH, 2003).

54. Barry, D. Effect of nonuniform boundary conditions on steady flow in saturated homogeneous cylindrical soil columns. *Advances in Water Resources* **32,** 522–531 (Apr. 2009).

55. Lewis, J. & Sjöstrom, J. Optimizing the experimental design of soil columns in saturated and unsaturated transport experiments. *Journal of contaminant hydrology* **115,** 1–13 (June 2010).

56. Kretzschmar, R. & Sticher, H. Colloid transport in natural porous media: influence of surface chemistry and flow velocity. *Physics and Chemistry of the Earth* **23,** 133–139 (1998).

57. Laumann, S., Micić, V., Lowry, G. V. & Hofmann, T. Carbonate minerals in porous media decrease mobility of polyacrylic acid modified zero-valent iron nanoparticles used for groundwater remediation. *Environmental pollution (Barking, Essex : 1987)* **179,** 53–60 (Aug. 2013).

58. Logan, J. *Transport modeling in hydrogeochemical systems, Chapter 2: Reaction-Advection-Dispersion Equation* (2001).

59. Scheidegger, A. E. General theory of dispersion in porous media. *Journal of Geophysical Research* **66,** 3273–3278 (Oct. 1961).

60. Toride, N., Leij, F. & Genuchten, M. V. *The CXTFIT code for estimating transport parameters from laboratory or field tracer experiments* tech. rep. 137 (U. S. Salinity Laboratory, Agricultural Research Service, Riverside, CA., 1995), 121.

61. Tufenkji, N., Miller, G. F., Ryan, J. N., Harvey, R. W. & Elimelech, M. Transport of Cryptosporidium oocysts in porous media: role of straining and physicochemical filtration. *Environmental science & technology* **38,** 5932–5938 (Nov. 2004).

62. Tufenkji, N. & Elimelech, M. Correlation equation for predicting single-collector efficiency in physicochemical filtration in saturated porous media. *Environmental science & technology* **38,** 529–536 (Jan. 2004).

63. Lince, F., Marchisio, D. L. & Barresi, A. a. Strategies to control the particle size distribution of poly-epsilon-caprolactone nanoparticles for pharmaceutical applications. *Journal of colloid and interface science* **322,** 505–515 (June 2008).

64. R Core Team. *R: A Language and Environment for Statistical Computing* R Foundation for Statistical Computing (Vienna, Austria, 2014).

65. Medrzycka, K. The effect of particle concentration on zeta potential in extremely dilute solutions. *Colloid and polymer science* **90,** 85–90 (1991).

66. Tantra, R., Schulze, P. & Quincey, P. Effect of nanoparticle concentration on zeta-potential measurement results and reproducibility. *Particuology* **8,** 279–285 (June 2010).

67. Dash, T. K. & Konkimalla, V. B. Poly--caprolactone based formulations for drug delivery and tissue engineering: A review. *Journal of controlled release : official journal of the Controlled Release Society* **158,** 15–33 (Mar. 2012).

68. De Queiroz, A. A. A., Franca, E. J., Abraham, G. a. & Roman, J. S. Ring-opening polymerization of epsilon-caprolactone by iodine charge-transfer complex. *Journal of Polymer Science Part B: Polymer Physics* **40,** 714–722 (Apr. 2002).

69. Voigt, a. *et al.* Electrokinetic properties of polymer and glass surfaces in aqueous solutions: experimental evidence for swollen surface layers. *Biomaterials* **4,** 299–304 (Oct. 1983).

70. Gu, Y. & Li, D. The $\zeta$-Potential of Glass Surface in Contact with Aqueous Solutions. *Journal of Colloid and Interface Science* **226,** 328–339 (June 2000).

71. Yang, X., Flynn, R., von der Kammer, F. & Hofmann, T. Quantifying the influence of humic acid adsorption on colloidal microsphere deposition onto iron-oxide-coated sand. *Environmental pollution (Barking, Essex : 1987)* **158,** 3498–506 (Dec. 2010).

72. Yang, X., Deng, S. & Wiesner, M. R. Comparison of enhanced microsphere transport in an iron-oxide-coated porous medium by pre-adsorbed and co-depositing organic matter. *Chemical Engineering Journal* **230,** 537–546 (Aug. 2013).

73. Ryan, J. & Gschwend, P. Effects of ionic strength and flow rate on colloid release: Relating kinetics to intersurface potential energy. *Journal of Colloid and Interface Science* **164,** 21–34 (1994).

74. Shen, C., Wang, L.-P., Li, B., Huang, Y. & Jin, Y. Role of Surface Roughness in Chemical Detachment of Colloids Deposited at Primary Energy Minima. *Vadose Zone Journal* **11** (2012).

75. Shellenberger, K. & Logan, B. E. Effect of molecular scale roughness of glass beads on colloidal and bacterial deposition. *Environmental science & technology* **36,** 184–189 (Jan. 2002).

76. Yao, K., Habibian, M. & O'Melia, C. Water and waste water filtration. Concepts and applications. *Environmental science & technology* **5,** 1105–1112 (1971).

77. Chen, J. Y., Ko, C.-H., Bhattacharjee, S. & Elimelech, M. Role of spatial distribution of porous medium surface charge heterogeneity in colloid transport. *Colloids and Surfaces A: Physicochemical and Engineering Aspects* **191,** 3–15 (Oct. 2001).

# Appendix

# A. Zusammenfassung

Heutzutage finden sich viele Polymere, wie zum Beispiel Poly($\epsilon$-caprolactone) (PCL), welche sich zur Herstellung von kapselähnlichen Strukturen eignen und als Transportmedium für einen bestimmten Wirkstoff eingesetzt werden können. Daraus ergeben sich wiederum veränderte Transporteigenschaften des Wirkstoffes, die sich auch auf die Mobilität im Untergrund auswirken können. Die vorliegende Studie wurde durchgeführt mit dem Ziel, den Einfluss von einer, auf PCL basierten, Nanokapsel (nanocarrier) auf den Transport des Herbizides (Wirkstoff) Atrazin im wassergesättigten Boden zu ermitteln. Dabei wurden die Auswirkungen von a) Einkapselung, b) erhöhte Ionenstärke und c) Ladungsheterogenität der Kollektoroberfläche auf Partikeldepositionsraten (deposition rate) und Anlagerungseffizienz (attachment efficiency) anhand von Säulenexperimenten untersucht. Die aus den Experimenten resultierenden Durchbruchskurven wurden mit Hilfe der Software STANMOD, die eine Convections-Dispersionsgleichung (CDE) löst, gefitted und analysiert. Der Transport und die Ablagung der Partikel wurde anschließend mit der kolloidalen Filtrationstheorie (CFT) beschrieben.

Sowohl das Fitten der Durchbruchskurven als auch die Anwendung der kolloidalen Filtrationstheorie zeigten keine direkte Auswirkung auf das Transport- und Ablagerungsverhalten durch die Einkapselung des Wirkstoffes. Dem gegenüber konnte eine Zunahme der Depositionsraten und Anlagerungseffizienz von etwa einer Größenordnung im Zusammenhang mit einer erhöhten Ionenstärke festgestellt werden. Allerdings blieb die tatsächlich beobachtete Ablagerungsmenge von Partikeln auf der Kollektoroberfläche gering ($C/C_0 = 0.92$). Das zusätzliche Beschichten der Kollektoroberfläche mit Ferrihydrit zur Erhöhung der Ladungsheterogenität zeigte wiederum keine Auswirkung auf die errechnete Depositionsrate und Anlagerungseffizienz.

Des Weiteren lässt sich aus den Resultaten der Modellierung im Zusammenhang mit einer vorhandenen Fraktion an größeren Partikel-Aggregaten ($\geq 1\mu$m), ein möglicher Einfluss von Ionenstärke auf den Partikeltransport durch Straining ableiten. Außerdem konnte gezeigt werden, dass sich die tatsächliche Freisetzungsrate des Wirkstoffes stark von den bisher angenommenen Raten aus vorangegangenen Studien unterscheidet [1]. Dies lässt vermuten, dass auch die tatsächliche Partikeldepositionsrate für den übrigen, noch eingekapselten Wirkstoff sehr viel höher ausfällt, als die Durchbruchskurven zunächst erwarten lassen. Besonders im Zusammenhang mit der erhöhten Ionenstärke scheint dies von Bedeutung zu sein. Die Ergebnisse weisen außerdem darauf hin, dass eine erhöhte Ober-

flächenladungsheterogenität entweder ein Remobilisieren des Nanopestizids, oder aber eine weitere Freisetzung des Wirkstoffes verhindern kann. Demnach scheint die Oberflächenladung für das Transportverhalten des Nanopestizids zumindest bedingt eine Rolle zu spielen.

Insgesamt wird der überwiegende Teil des Wirkstoffes in Lösung transportiert, weshalb ein Model für den gelösten Stofftransport besser geeignet erscheint um das Transportverhalten darzustellen, als die kolloidale Filtrationstheorie. Nichtsdestotrotz haben physikalisch-chemische Faktoren (z.B. Ionenstärke und Oberflächenladung) einen Einfluss auf den Transport und die Ablagerung des Nanopestizids. Weitere Experimente mit Produkten (Nanopestiziden), die eine geringere Freisetzungsrate des Wirkstoffes aufweisen werden benötigt, um den Einfluss von Nanokapseln auf den Transport des Wirkstoffes eindeutiger zu bestimmen.

# B. Curriculum Vitae

## Daniel Schweizer

*Curriculum Vitae*

## EDUCATION

**M.Sc. Environmental Science** Sept 2012 - Present

*University of Vienna*

Master Thesis: Transport of nanopesticides in saturated porous media

**BEF-China Summer School** March 2012

*BEF-China Project*

Topic: Scientific Writing in the Context of Biodiversity & Ecosystem Functioning; financed by DFG and Sino-German Center

**Exchange Student** Sept 2010 - May 2011

*University of British Columbia*

International Office exchange program; DAAD scholarship

**B.Sc. Forestry and Environmental Science** Oct 2008 - Aug 2012

*Albert-Ludwigs-University*

Minor: International Forestry; average grade: 1.5
Bachelor Thesis: Effect of tree composition on total soil phosphorus concentration in an evergreen broad-leaved forest of subtropical China; grade: 1.0

**High School Graduation** Sept 2003 - Jul 2006

*Richard-Fehrenbach-Gymnasium, Freiburg*

Average grade: 1.6

**Secondary School** Sept 1996 - Aug 2003

*Marie-Curie-Gymnasium, Kirchzarten*

## WORK EXPERIENCE

**Student Assistent** Sept 2011 - Aug 2012

*Forest Biometrics Department, Freiburg, Part-time*

FNet assistant: computer and network administration, software and hardware support.

**Internship** Sept - Oct 2011

*Molecular Ecology Department*
*Max-Plank-Institute for Chemical Ecology, Jena, Full-time*

qPCR, TPI essay, HPLC, GC-MS, RNA-extraction and isolation, Spectrophotometry

**Student Assistent** August 2011

*Silviculture Department, Freiburg, Full-time*

Setting up sample plots, collecting vegetation and soil data, digging and analysing soil profiles

**Internship** May 2011 - June 2011

*Department of Geography UBC, Vancouver, Full-time*

Preparing flume experiment and collecting data in the field: flow meter, laser tachymetry, sediment transport measurement

**Student Assistent** Jan 2011 - Apr 2011
*Department of Geography UBC, Vancouver, Part-time*
Assisting in experiment on fluvial hydrology: sieving, marking and preparing sediment fractions

**Construction Worker** Aug 2007 - Apr 2013
*Fa. Rievo, Full-time and Part-time*
Tennis courts and football fields; supervising, handling of machinery

**Climbing Instructor** Sept 2004 - Jun 2006
*Climbing Center Eigernord, Part-time*
Trainer of beginner groups, instructor and supervisior

## CIVIL SERVICE

**Substitutional Community Service** Aug 2006 - Aug 2007
*Jatun Sacha/ICYE, Ecuador*
Gained hands-on experiences in natural conservation projects of the mangroves and wet-forests

## SKILLS

| | |
|---|---|
| *Languages* | German (mother tongue)<br>English (fluent)<br>Spanish (fair) |
| *Software* | ArcGIS, LaTeX, R, SPSS, Modflow, Stanmod, Python, Linux (Ubuntu),Office |

## PREVIOUS FOREIGN TRAVELS

| | |
|---|---|
| *Sept 2010 - Jul 2011* | Canada, USA |
| *Dez 2007 - Apr 2008* | Thailand, India, Nepal |
| *Aug 2006 - Aug 2007* | Ecuador, Peru, Bolivia, Columbia |